frontiers | Frontiers in Cell and Developmental Biology

TYPE Original Research
PUBLISHED 23 September 2022
DOI 10.3389/fcell.2022.959094

Check for updates

OPEN ACCESS

EDITED BY
Paola Piomboni,
University of Siena, Italy

REVIEWED BY
Alexis Parada-bustamante,
University of Chile, Chile
Claudia Nora Tomes,
CONICET Mario H. Burgos Institute of Histology and Embryology (IHEM), Argentina

*CORRESPONDENCE
Priyanka Parte,
partep@nirrh.res.in

SPECIALTY SECTION
This article was submitted to Molecular and Cellular Reproduction, a section of the journal Frontiers in Cell and Developmental Biology

RECEIVED 01 June 2022
ACCEPTED 31 August 2022
PUBLISHED 23 September 2022

CITATION
Panchal D, Bhagwat S and Parte P (2022), N-Formyl-L-aspartate mediates chemotaxis in sperm via the beta-2-adrenergic receptor.
Front. Cell Dev. Biol. 10:959094.
doi: 10.3389/fcell.2022.959094

COPYRIGHT
© 2022 Panchal, Bhagwat and Parte. This is an open-access article distributed under the terms of the Creative Commons Attribution License (CC BY). The use, distribution or reproduction in other forums is permitted, provided the original author(s) and the copyright owner(s) are credited and that the original publication in this journal is cited, in accordance with accepted academic practice. No use, distribution or reproduction is permitted which does not comply with these terms.

N-Formyl-L-aspartate mediates chemotaxis in sperm *via* the beta-2-adrenergic receptor

Durva Panchal[1], Shweta Bhagwat[1,2] and Priyanka Parte[1]*

[1]Department of Gamete Immunobiology, ICMR-National Institute for Research in Reproductive and Child Health, Mumbai, Maharashtra, India, [2]Department of Obstetrics and Gynecology, Washington University School of Medicine, St. Louis, MO, United States

Chemotaxis is a highly conserved physiological event required for directed sperm movement during fertilization. Recently, studies from our laboratory have identified N-formyl-L-aspartate (NFA) as a sperm chemoattractant. NFA is a known agonist for the beta-2-adrenergic receptor (β-2-AR) that regulates cAMP production and Ca^{2+} mobilization in somatic cells. As these downstream signaling molecules are also reported to be involved in sperm chemotaxis, in the present study we investigated the putative mechanism/s by which NFA may mediate chemotaxis. Toward this, the expression and localization of β-2-AR in sperm were studied by Western blot and indirect immunofluorescence, respectively. The responses of sperm to various concentration gradients of NFA and ICI-118,551, a β-2-AR specific antagonist, were evaluated using the microfluidics device-based chemotaxis assay. The intracellular concentration of Ca^{2+}, on exposure to NFA, was analyzed using FURA-2 AM-based fluorimetric assay. Furthermore, the effect of NFA on sperm capacitation and acrosome reaction was evaluated using Western blot and immunofluorescence. NFA exhibited a bell-shaped dose-response curve typical of chemotaxis, with maximum response observed at 0.01M NFA, beyond which it was inhibitory; β-2-AR localization was seen on the sperm head and the mid-piece region of the flagella. Inhibition of sperm chemotaxis by ICI-118,551 confirms that sperm respond chemotactically to NFA *via* β-2-AR. Interestingly, at the concentration used for chemotaxis, NFA induced an increase in the intracellular Ca^{2+} but decreased cAMP in capacitating sperm. However, NFA *per se* did not induce capacitation as seen from the lack of effect on tyrosine phosphorylation and membrane potential of uncapacitated sperm. Acrosome evaluation of NFA-treated sperm using PSA-FITC staining showed no effect on the acrosome structure. Our data thus provide evidence indicating that NFA induces sperm chemotaxis and the chemotactic response of sperm to NFA from the ovulatory phase of oviductal fluid is mediated through the β-2-AR on sperm possibly via non-canonical signaling.

KEYWORDS

sperm chemotaxis, N-formyl-L-aspartate, beta-2-adrenergic receptor, capacitation, acrosome reaction, ICI-118, 551

Introduction

In mammals, during fertilization, only a small percentage of ejaculated sperm enter the oviduct and are actively guided by a combination of different guidance mechanisms before reaching the egg. One of the stages in gamete communication is sperm chemotaxis characterized by the release of chemical ligands from either the egg or cumulus cell or oviduct (Eisenbach, 1999). Several sperm chemoattractants such as RANTES (Isobe et al., 2002), atrial natriuretic peptide (Zhang et al., 2006; Bian et al., 2012), progesterone (Teves et al., 2009), allurin (Burnett et al., 2011), acetylcholine (Ko et al., 2012), and chemokine receptor CCR6 (Caballero-Campo et al., 2013) have been reported in various mammalian species. Sperm chemotaxis is maintained within a few millimeters in the vicinity of the egg and involves a complex series of molecular events that ensures the arrival of sperm toward an egg and fertilization (Guidobaldi et al., 2012).

For chemotaxis to occur in the vicinity of the egg, sperm must be functionally reprogrammed or capacitated in the female reproductive tract. This functional reprogramming enables the sperm to recognize the chemoattractants secreted either by the egg or its surrounding cells (Eisenbach, 1999). Sperm may have chemosensory receptors which likely get activated on encountering their cognate ligands. In mammalian species, olfactory receptors (Flegel et al., 2016) and taste receptors (Frolikova et al., 2020) have been of interest as molecular sensors for sperm-egg communication; however, their physiologically relevant ligands have not been identified yet. In general, receptor–ligand interaction in the ampulla of the oviduct leads to rapid downstream signal transduction resulting in sperm flagellar motor activation and regulation of motility to modulate its swimming path (Inaba, 2003). At molecular levels, sperm chemotaxis is associated with an increase in the intracellular concentrations of cAMP, cGMP (Shiba and Inaba, 2022), and Ca^{2+} (Oliveira et al., 1999; Teves et al., 2006). Despite identifying the chemical signals important for proper sperm function, our knowledge about the chemosensory receptors and their physiologically relevant ligands remains rudimentary.

Synthetically derived N-formylated peptides were first described to induce chemotaxis in human sperm (Gnessi et al., 1986a). There has been an increasing interest in these synthetically derived analogs due to their inherent potential to induce chemotaxis in neutrophils (Southgate et al., 2008a) and different bacterial species such as *E.coli* (Bi et al., 2013a) and *P.aeruginosa* (Bufe et al., 2015a). Recent studies from our group identified NFA as a chemoattractant using rat sperm. NFA levels were significantly higher in the ovulatory phase of oviductal fluid than in the pre-ovulatory phase (Bhagwat et al., 2021a). This is an integrative study deciphering the possible mechanism of NFA-mediated sperm chemotaxis. Furthermore, we also explored whether NFA could influence other crucial events in sperm such as capacitation and acrosome reaction. The findings of this study will aid in understanding the role of NFA and other putative chemoattractants in enhancing the fertilizing ability of sperm.

Materials and methods

Chemicals and reagents

Dulbecco's Modified Eagle Medium (DMEM) containing 4.5 g/L D-glucose, L-glutamine, 25 mM HEPES without phenol red, dimethylsulphoxide, Fura-2 AM, pluronic F-28, Triton X-100, $CaCl_2$, $MnCl_2$, and antagonist ICI-118,551, and 2-D quant kit were obtained from Sigma- Aldrich, USA. Chemicals used in the preparation of 2-D cell lysis buffer and sodium dodecyl sulfate-polyacrylamide were from HiMedia, India. NFA was procured from PureSynth Research Chemicals, Canada. The Femto-Plus Chemiluminescence detection kit and pre-stained protein markers were acquired from Thermo Fisher Scientific, USA. EDTA-free protease and broad-spectrum phosphatase inhibitor cocktail including Tyr, Ser/Thr phosphatases were obtained from Roche, Germany. The antibodies used in this study were as follows: rabbit anti-β-2-AR antibody purchased from BoosterBio, USA; mouse anti-α-tubulin antibody, mouse phosphotyrosine antibody, and PSA-FITC obtained from Sigma Aldrich, USA; HRP- and FITC-conjugated swine anti-rabbit and goat anti-mouse antibodies were from Dako-Agilent, USA.

Ethics approval

Adult male Wistar rats, 3–4 months of age were used in this study. Three rats were housed per cage and maintained in an atmosphere of 14 h light and 10 h dark in the animal breeding facility at the National Institute for Research in Reproductive and Child Health (ICMR-NIRRCH). Food and water were provided *ad libitum*. All the animal care practices and experimental procedures were approved by the Institutional Animal Ethics Committee (IAEC) of ICMR-NIRRCH.

Sperm preparation

The cauda epididymis of 3-months old sexually mature male rats were excised in sterile tubes containing DMEM, and sperm were allowed to swim up by incubation at 37°C for 15 min in an atmosphere of 5% CO_2 and 95% air. The supernatant containing actively motile sperm was carefully separated and evaluated for concentration and motility. Sperm concentrations were greater than 50×10^6 cells/mL and motility was over 70%. 2×10^6 cells were then incubated in DMEM alone or for capacitation in DMEM supplemented with 2.5% bovine serum albumin (BSA) for 2.5 h at 37°C in an atmosphere containing 5% CO_2 and 95%

air (Bhagwat et al., 2018). Motility was assessed at 0 and 2.5 h of capacitation incubation and at the end of the chemotaxis experiment to ensure that the motility was more than 60% throughout the experiment. The effect of antagonist ICI-118,551 on chemotaxis was evaluated after exposing capacitating sperm to the antagonist for 30 min before the chemotaxis assay.

Sperm motility assay

Sperm motility was analyzed using a motility chamber prepared as reported previously (Bhagwat et al., 2018). Briefly, the motility chamber was prepared by wrapping four layers of scotch tape on a glass slide (3 cm apart, height ~200 microns). A suspension of 1:50 diluted sperm was loaded into a motility chamber pre-warmed at 37°C and a coverslip (22 × 40 mm) was placed on the slide. The slide was mounted on an optical microscope equipped with an sCMOS camera. Sperm motility was analyzed by capturing videos at ×10 magnification (8-bit MPTIFF, 2058 × 2018 pixels at 45 fps for 10 s). For each experimental set, ~10 movies each of 10 s durations were recorded and at least 200 sperm were analyzed. Sperm viability was checked by staining sperm with 0.5% Eosin Y. Those that stained pink were counted as non-viable.

Sperm chemotaxis assay

Sperm chemotaxis was analyzed using the microfluidic device developed in-house and as reported previously (Bhagwat et al., 2018). Briefly, for chemotaxis assay, the device was set in a chamber maintained at 37°C mounted on the stage of a laser scanning confocal microscope (LSCM; LSM780, Carl Zeiss Microscope, Thornwood, NY, USA). Different concentrations of NFA (0.001, 0.005, 0.01, or 0.02 M) were allowed to form gradients in DMEM in the test channels of the device by maintaining a constant flow rate of 1 μL/min using a syringe pump (NE-1000, New Era Pump System Inc., Farmingdale, NY, USA). Similar incubations in media alone served as the control in every experiment. Next, 2×10^6 capacitating sperm were added to the cell reservoir. After stabilization of the flow and gradient for 10 min, sperm motion in the test channels was captured at ×10 magnification using an sCMOS camera (8-bit MPTIFF, 2058 × 512pixel) at 90 fps for 15 sec. During each experimental set, ~30 movies each of 15s duration were recorded and at least 200 sperm were analyzed.

Estimation of chemotaxis

Chemotaxis was determined by assessing the changes in sperm motion in response to gradients formed by NFA in the test channel. The total number of sperm moving toward and against the gradient concentrations of 0.001, 0.005, 0.01, or 0.02 M NFA and DMEM, was estimated. The percentage of sperm swimming in the ascending direction of the gradient was calculated for each gradient concentration of NFA and compared to its respective DMEM control. The speed bias of sperm swimming toward a chemoattractant gradient was assessed by calculating the straight-line velocity (VSL). Individual sperm traveling in the test channel were tracked for their VSL using the manual tracking plugin in Image-J software (v1.50b; NIH, USA). The net distance (d) was calculated using the formula $d = \sqrt{(x_2 - x_1)^2 + (y_2 - y_1)^2}$ where (x_1, y_1) and (x_2, y_2) are the x and y coordinates of initial and final position, respectively, obtained while tracking individual sperm and was normalized to time (Schneider et al., 2012).

Protein extraction and western blotting

Caudal sperm were obtained as described earlier in this section. Sperm pellets were washed thrice with 0.1 M phosphate buffer saline (PBS), pH 7.2, by centrifugation at 800 *g* for 30 min at 4°C. Sperm lysates were prepared by re-suspending the pellets in 2D-lysis buffer containing 7 M urea, 2 M thiourea, 4% CHAPS, and 30 mM Tris, supplemented with protease and phosphatase inhibitors, for 18 h at 4°C, followed by homogenization using a Fast-prep-24 Homogenizer (MP, Biomedicals, Irvine, United States). The homogenized lysates were incubated for 30 min at 4°C followed by centrifugation at 1,000 *g* for 30 min at 4°C to collect the supernatant. The total protein concentration in the supernatant was estimated using the 2-D quant protein estimation kit. A total of 40 μg of the protein lysate was electrophoresed on 10% SDS-PAGE and transblotted to a nitrocellulose membrane (Pall Biosciences, United States). Nonspecific binding was blocked by incubating the membranes with 5% non-fat dried milk (NFDM) in Tris-buffered saline containing 0.1% Tween (TBST) for β-2-AR, or with 5% BSA in 0.1% TBST for phospho-tyrosine, at room temperature (RT) for 1 h. The membranes were incubated overnight at 4°C with either anti-β-2-AR antibody diluted 1:500 in TBST containing 1% NFDM (TBST-NFDM) or with anti-phosphotyrosine antibody diluted 1:1,000 in TBST containing 1% BSA (TBST-BSA). The membranes were washed three times for 5 min each in 0.1% TBST and incubated for 1 h at RT with either 1:3000 HRP-conjugated swine anti-rabbit or 1:5000 HRP-conjugated goat anti-mouse secondary antibodies diluted in TBST-NFDM or TBST-BSA, respectively. The membranes were then washed five times for 5 min each and the protein bands were detected using a chemiluminescence-based detection system. To account for protein load, the same blots were probed with 1:10,000 diluted goat anti-α-tubulin antibody diluted in TBST-NFDM after stripping off the bound specific antibodies by two washes for

10 min each with stripping buffer, pH 2.2, containing 0.2 M glycine, 3.5 mM SDS, 8 mM Tween-20, and 0.3 mM HCl. The membranes were then washed twice for 10 min each with 0.1 M TBS, followed by two washes of 5 min each with 0.1% TBST and finally, two washes with 0.1 M TBS for 10 min each. The membranes were processed further as described previously. The lane intensity of tyrosine-phosphorylated proteins was measured and normalized to the band intensity of the loading control α-tubulin and the data were quantified using Image-J software (NIH, US).

Indirect immunofluorescence

For IIF, sperm were resuspended in 0.1 M PBS, such that their final concentration was 2×10^6 cells/mL. A total of 10 µL of the sperm suspension was spread uniformly on 0.1% poly-L-lysine-coated glass slides, air-dried and fixed in 95% (w/v) acetone for 3 min followed by 95% (w/v) methanol for 1 min at 4°C. Cells were either used intact or permeabilized with 0.1% (w/v) Triton-X-100 and 1% (w/v) glacial acetic acid. Non-specific binding was eliminated by incubating the slides with 3% BSA for 1 h at RT. The slides were then incubated overnight at 4°C with rabbit anti-β-2-AR, diluted 1:50 with 0.1 M PBS. The slides were washed three times for 10 min each with 0.1 M PBS at RT under slow rocking conditions. The slides were then incubated with 1: 200 diluted FITC-conjugated swine anti-rabbit antibody and 0.01% DAPI (Sigma Aldrich, United States) for 1 h at RT in dark. Finally, the slides were washed thrice for 10 min each with 0.1 M TBS and mounted using Prolong-Gold (Sigma Aldrich, US). The slides were examined using an epifluorescence microscope (LSCM; LSM780, Carl Zeiss Microscope, Thornwood, NY, United States).

PSA-FITC staining

The effect of NFA on the acrosome of capacitating sperm was assessed by the PSA-FITC staining method. 2×10^6 sperm were allowed to capacitate by incubating them in DMEM supplemented with 2.5% BSA, for 2.5 h at 37°C in an atmosphere of 5% CO_2 and 95% air. After incubation, the sperm were treated with either 0.01 M NFA or 10 µM progesterone for 30 min at 37°C in an atmosphere of 5% CO_2 or 95% air. Capacitated sperm incubated with DMEM for 30 min served as controls. Next, 10 µL of each sample was uniformly spread on 0.1% poly-l-lysine-coated glass slides, air-dried, fixed with 95% (w/v) acetone for 3 min followed by 95% (w/v) methanol for 1 min, and incubated with 3% PSA-FITC (3 µg/ 100 µL) in dark for 30 min at RT. The slides were then washed thrice for 10 min each with 0.1 M PBS and mounted using Prolong-Gold. The slides were examined using an epifluorescence microscope. For each sample, 150–200 sperm were analyzed and classified as acrosome intact (AI) for sperm showing intense fluorescence over the sperm head indicative of an intact acrosome, or as Acrosome reacted (AR) for those with low or absent fluorescence over the head, typically seen in an acrosome-reacted sperm.

Intracellular Ca^{2+} measurement in sperm

The intracellular Ca^{2+} $[Ca^{2+}]_I$ levels in sperm were measured using Fura-2AM, following an established protocol (Bhagwat et al., 2021a). Briefly, 10^7 capacitating sperm were incubated in DMEM with or without the β-2-AR antagonist ICI-118,551 for 30 min at 37°C. They were then loaded with 5 µM Fura-2AM and incubated at 37°C for 45 min in an atmosphere of 5% CO_2 and 95% air with intermediate mixing. After incubation, the dye-loaded cells were washed thrice with DMEM by centrifugation at 600 *g* for 30 min at 37°C to remove unbound Fura-2AM. 2×10^6 dye-loaded sperm were then resuspended in Ca^{2+} containing Tyrode's buffer with 0.001, 0.005, and 0.01 M NFA in a 96-well black polystyrene microtiter plate (Labsystems, India) at a final volume of 200 µL. Sperm were evenly resuspended by mixing for 30 s in the spectrofluorimeter. Fura-2AM excitation was set at 380 and 340 nm to determine the free and bound calcium, respectively. Fluorescence readings were recorded at intervals of 15 s for 15 min and cells were lysed with 1% Triton-X-100 followed by the addition of 3 mM $CaCl_2$ for F_{max} and 2 mM $MnCl_2$ for F_{min}. The $[Ca^{2+}]_I$ concentration was calculated using the formula $[Ca^{2+}]_I = \frac{Kd\ (F-Fmin)}{(Fmax-F)}$ where K_d is the dissociation constant, F is the fluorescence reading calculated as the ratio of 340/380, and F_{max} and F_{min} are the maximum and minimum calcium levels, respectively, over the incubation period of 15 min.

Intracellular cAMP measurement in sperm

The intracellular levels of cAMP in sperm were measured using direct competitive ELISA (cAMP assay kit, ADI-900-066A, Enzo life science, US). Next, 10^6 cells were incubated with either DMEM, DMEM supplemented with 2.5% BSA, or 0.01 M NFA at 37°C for 2.5 h in an atmosphere of 5% CO_2 and 95% air. After incubation, 100 µL of each cell sample was added to 200 µL of 0.1 N HCl and homogenized using a Fast-prep-24 homogenizer. The cell lysate was centrifuged at 600 g for 5 min at 37°C. The resultant supernatant was then used for competitive ELISA as per the kit protocol.

Sperm membrane potential measurement

The fluorimetric measurement of sperm membrane potential was carried out using a voltage-sensitive dye, $DiSC_3$, using a

published protocol (Baro Graf et al., 2020). Briefly, 10^7 sperm were incubated for 2.5 h in either DMEM supplemented with 1% BSA, DMEM supplemented with 2.5% BSA, or with 0.01 M NFA and 1% BSA. From each group, 2×10^6 sperm/200 µL were transferred to a black 96-well polystyrene microtiter plate and loaded with 1 µM $DiSC_3$ solubilized in 1% DMSO. The plate was transferred to a spectrofluorimeter with gentle mixing for 10 s and the fluorescence was measured at 37°C at excitation/emission wavelengths of 620/670 nm, respectively. Internal calibration for each determination compensates for the variable that can influence the absolute fluorescence values. Calibration of the $DiSC_3$ assay was carried out using 1 µM valinomycin dissolved in 1% DMSO and sequential addition of 1.67, 3.40, 5.95, and 10.20 µL of 2 M KCl. The theoretical Em values were calculated using the Nernst equation considering 120 mM as the internal K^+ concentration. The final membrane potential was calculated by linearly interpolating the theoretical Em values against the arbitrary fluorescence units at each time point.

Statistical analysis

Statistical analysis was done using GraphPad Prism 9.0.4 software (GraphPad Software Inc.). Results are expressed as mean ± SD or SEM. One-way ANOVA was used to determine the difference between the groups with Dunn's post hoc test for multiple comparisons. When the experiments had more than one variable, two-way ANOVA was used for statistical analysis. The difference was considered to be statistically significant when the *p*-value was less than or equal to 0.05.

Results

NFA demonstrates a bell-shaped dose-dependent response typical of a chemoattractant

Recent studies by our group reported sperm chemotaxis at a concentration gradient of 0.01 M NFA (Bhagwat et al., 2021a). In the present study, we evaluated the response of sperm to concentration gradients lower and higher than 0.01 M NFA using microfluidic device-based chemotaxis assays. To examine whether and how higher or lower concentration gradients of NFA influenced the sperm numbers entering the transverse channel, we calculated the percentage of sperm moving toward and against gradients formed by 0, 0.001, 0.005, 0.01, and 0.02 M NFA. The percentage of sperm responding positively to NFA increased as the gradients got steeper up to a concentration of 0.01 M, beyond which, i.e., at 0.02 M NFA, there was a decrease observed (Figure 1A). The results demonstrated a bell-shaped dose-dependent response curve (typical of chemotactic cell behavior), with significant response seen at a concentration gradient of 0.01 M NFA in comparison to the DMEM control (**$p < 0.01$) and in comparison, to a gradient of 0.001 M NFA (**$p < 0.05$).

Increase was also observed in the mean straight-line velocity (VSL) of sperm moving toward increasing concentration gradients of 0.001, 0.005, and 0.01 M, with statistical significance observed at 0.005 M (**$p < 0.01$) and 0.01 M (***$p < 0.005$) as compared to the DMEM control. A significant decrease in the mean VSL was seen at a gradient of 0.02 M NFA (**$p < 0.01$) as compared to that seen with 0.01 M NFA. The VSL at the 0.02 M gradient of NFA was comparable to that seen in the DMEM control, 0.001 M, and 0.005 M NFA (Figure 1B). A frequency distribution plot for sperm velocities at different concentrations of NFA showed that the sperm population exposed to a gradient formed by 0.01 M NFA had a higher percentage of sperm moving at the VSL range 81–160 and >160 µm/sec and a lower percentage of sperm in the VSL range of <40 and 41–80 µm/sec as compared to other concentrations (Figure 1C). Data for each experimental set are provided in Supplementary Table S1.

β-2-AR is present on the sperm surface

NFA is patented as a β-2-AR agonist (US-2005261338-A1, US-2007179179-A1, and US-2008269344-A1). Additionally, N-formylated peptides have been suggested to demonstrate chemotaxis toward human sperm (Gnessi et al., 1986a), neutrophils (Naccache et al., 2000a; Southgate et al., 2008a), and bacterial species such as *Pseudomonas aeruginosa* (Ijiri et al., 1994a; Bufe et al., 2015a) and *E. coli* (Bi et al., 2013a). Studies from our group have reported significantly increased concentrations of NFA in the ovulatory phase compared to the pre-ovulatory phase-rat oviductal fluid. Therefore, we first investigated the presence of β-2-AR in rat sperm. By Western blot analysis, a specific band at ~72 kDa was detected for β-2-AR in uncapacitated and capacitating sperm lysates (Figure 2A). Similarly, evaluation of human sperm lysates detected proteins of molecular weights ~95 and ~55 kDa, in addition to the ~72 kDa band (Supplementary Figure S1). Furthermore, we studied the localization of β-2-AR in uncapacitated and capacitated sperm using IIF. A positive signal for β-2-AR was seen on the head and the mid-piece region of sperm, with decreasing or fainter fluorescence on the principal piece and end piece. On permeabilization of sperm with 0.1% Triton X-100 and 1% glacial acetic acid, the intensity of the fluorescence signal diminished indicating that β-2-AR is present on the sperm surface. Although the immunofluorescence data are not quantitative, there was no discernible difference in β-2-AR intensities between capacitated and uncapacitated sperm (Figure 2B).

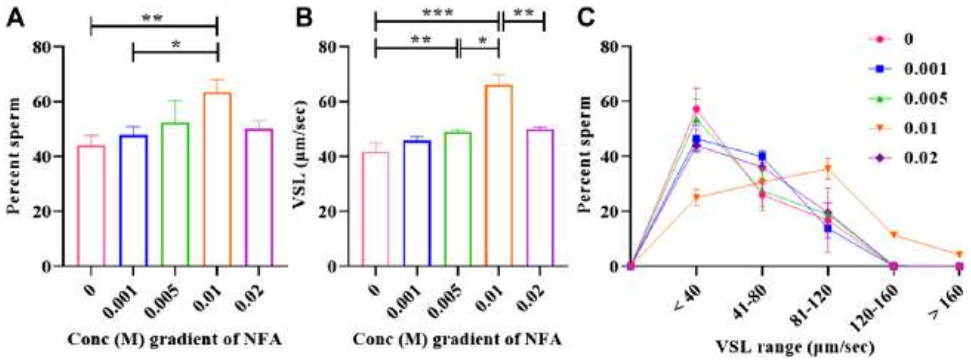

FIGURE 1
Bell-shaped dose-response of sperm to NFA. Chemotaxis was studied using the microfluidics device at gradient concentrations of 0, 0.001, 0.005, 0.01, and 0.02 M NFA after capacitating sperm for 2.5 h. Sperm directionality is represented as the percentage of sperm entering the transverse channel and moving toward the ascending concentration gradient of NFA **(A)**, sperm VSL **(B)**, and frequency distribution of sperm VSL in response to increasing gradients of NFA **(C)**. Each column represents mean ± SEM for the respective gradient tested (***p < 0.005; **p < 0.01; *p < 0.05). The results presented are cumulative from three independent experiments.

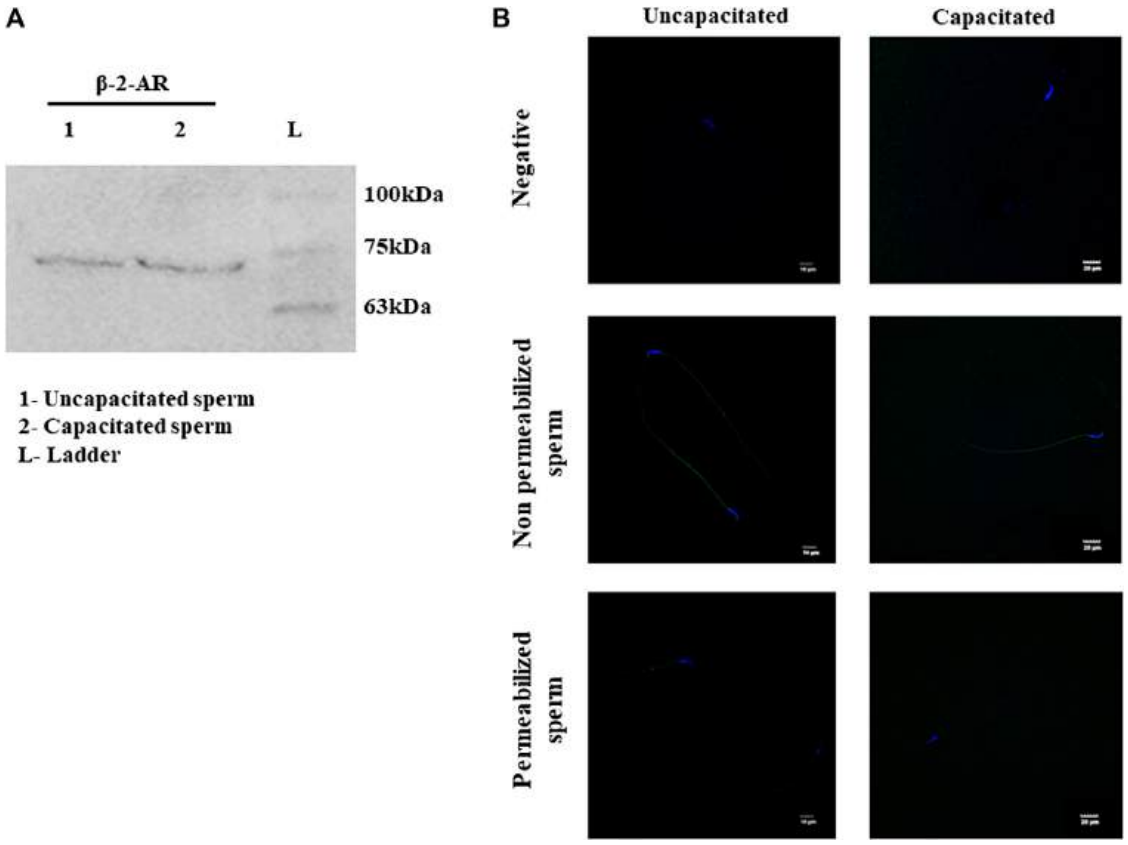

FIGURE 2
Expression and localization of β-2-AR in sperm. Lysates of uncapacitated and capacitated sperm were electrophoresed on 10% SDS PAGE and probed for β-2-AR by Western blot analysis, using antibodies specific for β-2-AR **(A)**. The complete blots and their ponceau profiles are provided in Supplementary Figure S1. IIF localization shows the presence of β-2-AR (green) in uncapacitated and capacitated intact and permeabilized sperm **(B)**. Nuclei of sperm were stained with DAPI (blue). The negative control shows sperm incubated with only the secondary antibody. This experiment was done in triplicates using sperm from three individual rats.

TABLE 1 Percent motility of sperm on exposure to different concentrations of ICI-118,551.

Time (min)	DMEM	0.01 M NFA	0.01 μM ICI-118,551	0.1 μM ICI-118,551	1 μM ICI-118,551
0	58.90 ± 0.46	61.61 ± 0.51[a]*	58.75 ± 0.20[b]*	57.73 ± 0.96	57.42 ± 1.29
15	51.60 ± 1.40	59.36 ± 1.12[a]*	54.12 ± 1.32	47.50 ± 2.04[a]*	44.96 ± 0.57[a*,b]**
30	47.82 ± 0.95	57.74 ± 0.61[a]**	51.75 ± 2.24	45.32 ± 0.95[a]*	41.71 ± 0.88[a**,b]***
45	41.26 ± 0.57	52.89 ± 1.34[a]*	45.44 ± 2.39	38.50 ± 0.54[a]*	33.02 ± 1.20[a*,b]***

[a]significant compared to DMEM.
[b]significant compared to 0.01 M NFA.
(*$p < 0.05$; **$p < 0.005$; ***$p < 0.001$).

TABLE 2 Percent viability of sperm on exposure to different concentrations of ICI-118,551.

Time (min)	DMEM	0.01 M NFA	0.01 μM ICI-118,551	0.1 μM ICI-118,551	1 μM ICI-118,551
0	66.33 ± 3.85	66.00 ± 1.63	65.66 ± 3.39	65.33 ± 3.30	64.33 ± 4.19
15	64.00 ± 2.44	63.33 ± 2.62	66.33 ± 4.11	64.66 ± 2.62	55.00 ± 2.82
30	63.66 ± 2.62	62.66 ± 0.94	61.66 ± 2.62	65.00 ± 2.94	53.00 ± 5.71 [a]*
45	57.33 ± 0.47	64.00 ± 2.44	60.00 ± 0.81	56.66 ± 1.70	44.67 ± 3.39 [a]*

[a]significant compared to 0.01 M NFA.
(*$p < 0.05$).

β-2-AR antagonist blocks NFA-mediated sperm chemotaxis

Having obtained evidence for the presence and location of β-2-AR on sperm, we next looked for evidence on whether or not NFA mediates its chemotactic effect *via* β-2-AR, using the β-2-AR-specific antagonist ICI-118,551. Toward this, the effective concentration of ICI-118,551 that was not lethal to sperm *per se* was determined by quantifying sperm motility and viability immediately and after 15, 30, and 45 min post-incubation with 0.01, 0.1, and 1 μM ICI-118,551. The significance of differences between treatment groups was analyzed by 2-way ANOVA. Sperm motility was significantly increased after exposure to 0.01 M NFA compared to the DMEM control at all the time points tested. A slight yet significant reduction was seen with 0.01 μM ICI-118,551 compared to that with NFA immediately on incubation but not at later time points; however, it was comparable to the media control. At higher concentrations of ICI-118,551, it significantly and progressively reduced from 15 min onward with respect to that seen with DMEM and NFA (Table 1). On the other hand, sperm viability was compromised after 30 and 45 min incubation only with 1 μM ICI-118551 (Table 2). On the basis of these data, 0.01 μM ICI-118551 was identified as a suitable concentration and used for subsequent experiments to test whether it inhibits NFA-mediated chemotaxis.

Chemotaxis to NFA in the presence of 0.01 μM ICI-118,551 was assessed by incubating sperm for 2.5 h with BSA to capacitate them followed by incubation with or without 0.01 μM ICI-118,551 for 30 min and then determining their response to a gradient of 0.01 M NFA in the chemotaxis assay. The percentage of sperm entering the transverse channel toward the ascending gradient of 0.01 M NFA and their VSL was determined. After treatment with 0.01 μM ICI-118,551, the percentage of sperm responding to an ascending gradient of 0.01 M NFA significantly decreased as compared to the untreated group (**$p < 0.01$) (Figure 3A). A significant decrease (**$p < 0.01$) was also observed in the mean VSL of sperm moving toward the ascending gradient of NFA, after treatment with the antagonist (Figure 3B). A frequency distribution plot for the VSL of the sperm population exposed to the antagonist showed a significant change in sperm VSL. In the absence of pre-treatment with ICI-118,551, a higher percentage of sperm responded to NFA with VSL 81-120 and >120 μm/sec compared to those seen with DMEM alone. However, the percentage of sperm responding to NFA with VSL 81-120 and >120 μm/sec was significantly lower in sperm pre-treated with the antagonist (Figure 3C). Data for each experimental set are provided in Supplementary Table S2.

NFA increases $[Ca^{2+}]_I$ levels

To determine the influence of 0.01 M NFA on $[Ca^{2+}]_I$, Fura-2AM-loaded capacitating sperm were incubated with 0.001, 0.005, and 0.01 M NFA and the fluorescence intensity was

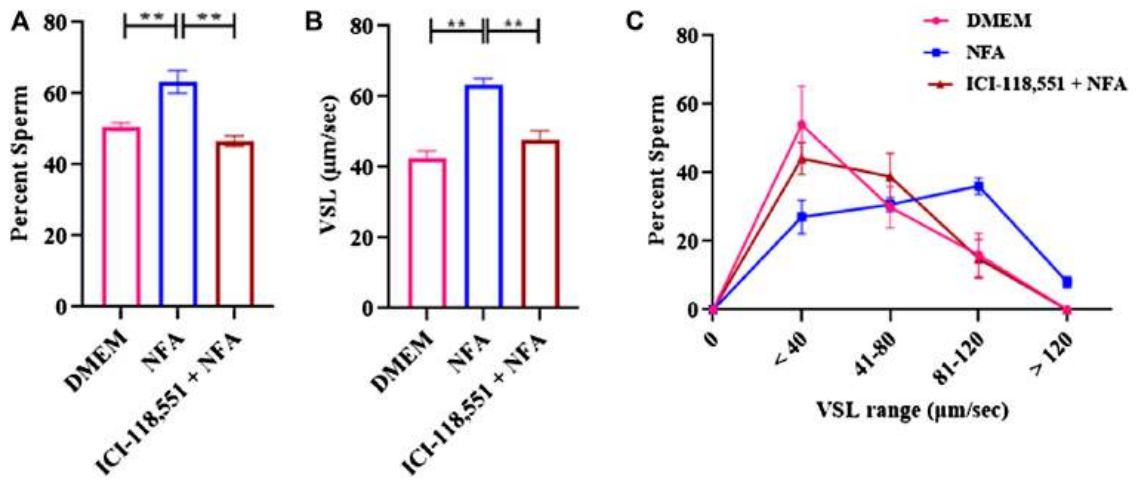

FIGURE 3
β-2-AR antagonist blocks sperm chemotactic responses to NFA. The effect of β-2-AR antagonist on sperm chemotaxis was studied after 30 min exposure of capacitating sperm to 0.01 µM ICI-118,551 before exposing them to a gradient of 0.01 M NFA and evaluating chemotaxis in the microfluidics device. Sperm directionality is presented as the percentage of sperm moving toward the ascending concentration gradient of NFA in the transverse channel **(A)**; sperm VSL **(B)**; and frequency distribution of sperm VSL under these conditions **(C)**. Each column represents mean ± SD (**p < 0.01). The results represented are cumulative from three independent experiments.

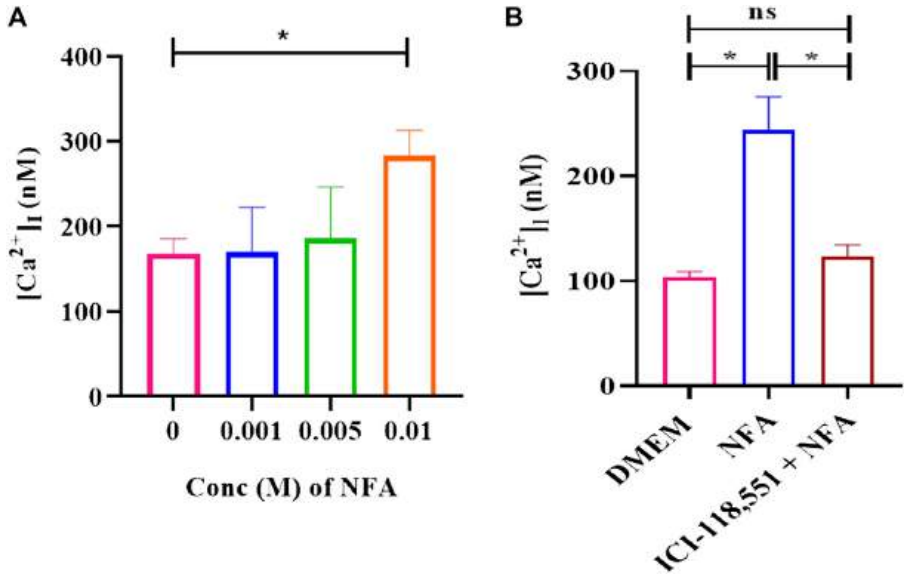

FIGURE 4
NFA increases $[Ca^{2+}]_I$ levels in capacitating sperm. $[Ca^{2+}]_I$ was assessed on exposure of capacitating sperm to 0.001, 0.005, and 0.01 M NFA using Fura-2 AM-based assay. Fura-2AM-loaded capacitating sperm were stimulated with the stated concentrations of NFA and the corresponding F-max and F-min values were recorded after the addition of 1% Triton X-100. Excitation of the dye with bound and unbound calcium was measured at 340 and 380 nm, respectively, and fluorescence emission at 500 nm. The figure shows a graph of $[Ca^{2+}]_I$ at different concentrations of NFA **(A)**. The effect of the β-2-AR antagonist on $[Ca^{2+}]_I$ was studied after 30 min exposure of capacitating sperm to 0.01 µM ICI-118,551 before exposing them to 0.01 M NFA **(B)**. The results presented are cumulative from three experiments. Values are expressed as mean ± SEM. *p < 0.05.

measured to calculate the levels of $[Ca^{2+}]_I$. A dose-associated increase in $[Ca^{2+}]_I$ was observed in sperm exposed to 0.001, 0.005, and 0.01 M NFA, with the increase being significant at 0.01 M NFA compared to DMEM (*$p < 0.05$) (Figure 4A). This increase was abrogated when capacitating sperm treated with ICI-118,551 for 30 min were exposed to 0.01 M NFA. They were

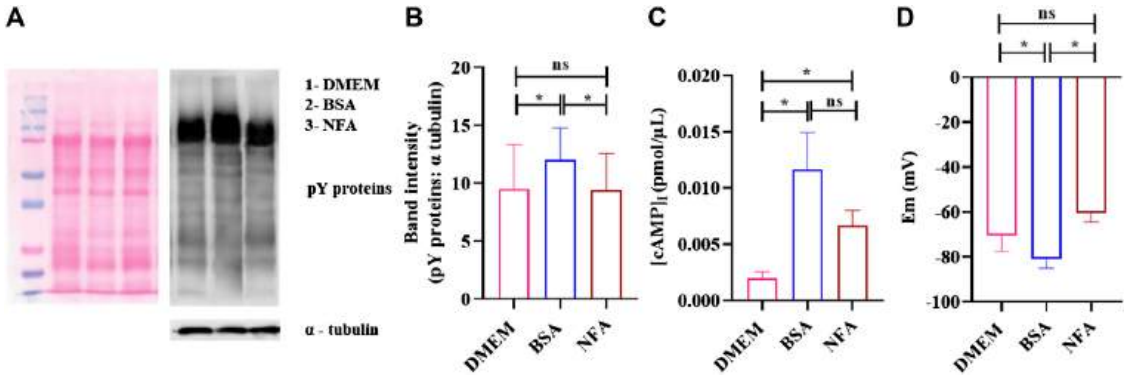

FIGURE 5
NFA at chemotactic concentrations does not induce capacitation. Protein tyrosine phosphorylation, $[cAMP]_I$, and membrane potential was determined in sperm incubated in DMEM, 2.5% BSA, or 0.01 M NFA for 2.5 h. Protein tyrosine phosphorylation was detected by Western blot analysis using mouse anti-phosphotyrosine and HRP-conjugated goat anti-mouse as primary and secondary antibodies, respectively. A representative image of the Western blot for pY proteins (right) and its corresponding ponceau-stained blot (left) are shown **(A)**. The band intensities of tyrosine-phosphorylated proteins normalized to that of the loading control, α- tubulin, are shown **(B).** $[cAMP]_I$ was assessed by competitive ELISA. Absorbance was measured at 480 nm. The figure shows a graph of $[cAMP]_I$ levels under different conditions **(C)**. The sperm membrane potential was determined using DiSC3-based fluorimetric assays. Represented are absolute Em (mV) values of the sperm membrane after treatment **(D)**. Values represent the mean ± SD of three independent experiments. (*p < 0.05; **p < 0.01).

comparable to the levels in capacitating sperm (Figure 4B). Data of each experimental set are provided in Supplementary Tables S3A,B.

NFA does not induce capacitation or acrosome reaction in sperm

Sperm capacitation and acrosome reaction are prerequisites for successful fertilization. We explored the effect of 0.01 M NFA on these parameters. The effect on capacitation was evaluated by determining the extent of tyrosine phosphorylation, membrane potential, and levels of intracellular cAMP in sperm after exposure to NFA. For all these parameters, 2×10^6 sperm were incubated for 2.5 h in DMEM alone, or DMEM supplemented with either 2.5% BSA or 0.01 M NFA. Incubations with BSA served as a positive control for capacitation. The extent of tyrosine phosphorylation was detected using a specific anti-phosphotyrosine antibody by Western blot analysis (Figure 5A) and IIF. Sperm did not show any significant difference in the phosphotyrosine intensity after 2.5 h of incubation with NFA (Figure 5B). Interestingly, detection by IIF showed a slight yet significant decrease in the percent of sperm with tail fluorescence (Supplementary Figure S2).

$[cAMP]_I$ was measured using competitive ELISA. The $[cAMP]_I$ increased after treatment with NFA (*$p < 0.05$*), reaching a concentration of 0.006 pmol/μL as against 0.002 pmol/μL seen on incubation with DMEM (Figure 5C). Hyperpolarization of the sperm plasma membrane was also studied using a fluorimetric population assay to determine the absolute membrane potential (Em). Em was determined using a positively charged carbocyanine probe $DiSC_3$. Sperm incubated with BSA displayed Em of -81.17 ± 3.09 mV as against -70.55 ± 5.68 mV seen in DMEM incubation. NFA was least effective in inducing capacitation-associated hyperpolarization with an Em of -60.47 ± 3.20 mV. The Em of sperm treated with 0.01 M NFA was found to be comparable to that seen with DMEM (Figure 5D).

To evaluate whether NFA induces an acrosome reaction, 2×10^6 capacitating sperm were incubated with 0.01 M NFA for 1 h and then assessed by PSA-FITC staining. Sperm incubated with 10 μM progesterone were used as a positive control. At the end of the incubation period, the motility was evaluated and was observed to be greater than 70% in each group. PSA-FITC staining uses fluorescein-conjugated lectin to distinguish sperm with an intact acrosome (AI) from those with a reacted acrosome (AR). Sperm with intact acrosomes display uniform and bright fluorescence whereas acrosome reacted sperm show less fluorescence in the sperm head. The percentage of AR sperm in the NFA-treated suspension was comparable to that seen with DMEM. Incubations with 10 μM progesterone showed a significantly higher percentage of AR sperm than expected (Figure 6).

Discussion

In mammals, sperm chemotaxis is an important guidance mechanism directing sperm to the egg. Human sperm (Gnessi et al., 1986a), neutrophils (Naccache et al., 2000a; Southgate et al.,

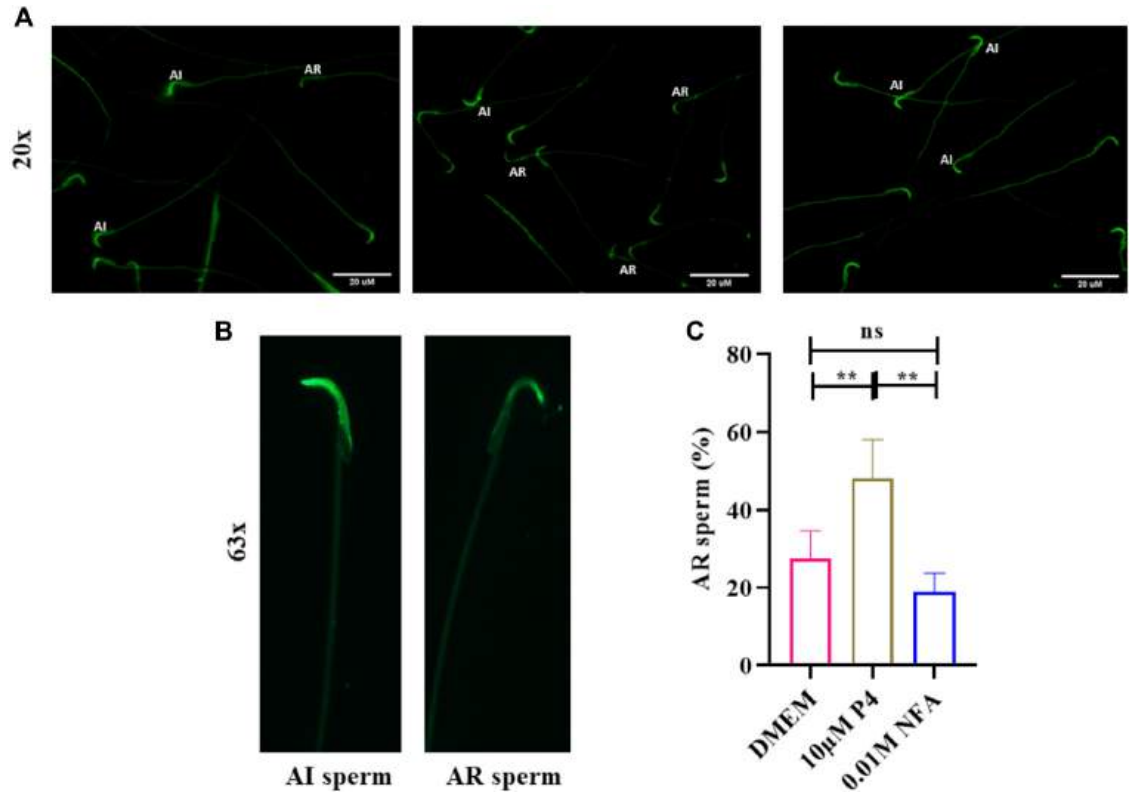

FIGURE 6
NFA does not induce acrosome reactions in sperm. The acrosome reaction was evaluated by PSA-FITC staining. Sperm were incubated in DMEM, without or with 10 μM progesterone (P4), or 0.01 M NFA for 1 h after capacitation and subjected to PSA-FITC staining. After PSA-FITC staining, sperm were examined by epifluorescence microscopy. AR, acrosome reacted sperm; AI, acrosome intact sperm **(A,B)**. The percentages of acrosome reacted sperm were calculated by dividing the number of acrosome reacted sperm by the total number of sperm for each group **(C)**. Bars represent mean ± SD.

2008a), and bacterial species such as *Pseudomonas aeruginosa* (Ijiri et al., 1994a; Bufe et al., 2015a) and *E. coli* (Bi et al., 2013a) have all been reported to respond chemotactically to synthetically derived N-formylated peptides. Recent studies by our group have reported significantly higher levels of NFA in the ovulatory phase-oviductal fluid compared than in the pre-ovulatory phase. Additionally, we demonstrated it to be a sperm chemoattractant at 0.01 M concentration (Bhagwat et al., 2021a). In the present study, we investigated the response of sperm to gradients ranging from 0.001–0.02 M NFA using microfluidics-based chemotaxis assays. Whilst the percentage of sperm moving toward higher concentrations and their velocities increased concomitant to the gradient concentrations, it was highly significant at a gradient concentration of 0.01 M NFA. A significant increase in the percentage of sperm with a VSL range of 81–160 and >160 μm/sec was noted with 0.01 M NFA. At 0.02 M NFA, there was a drop (Figures 1A–C). This bell-shaped dose-response curve is characteristic of a chemoattractant. These observations indicate that sperm can sense increasing concentration gradients up to 0.01 M NFA; any further increase is detrimental, thereby suggesting the possibility that NFA is sensed by the sperm via some receptor and that higher concentrations of NFA probably saturate and desensitize the receptors, rendering the sperm unable to sense it resulting in a drop in velocities and, consequently, the number of chemotactic sperm.

We, therefore, investigated the cognate receptors for NFA on sperm. NFA has been patented as a β-2-AR agonist (US-2005261338-A1, US-2007179179-A1, and US-2008269344-A1). β-2-ARs are transmembrane glycoproteins containing eight alpha helices (3-extracellular and 5-intracellular) and are associated with a heterotrimeric G-protein (specifically a G-protein stimulatory subunit) (Yang et al., 2021). β-2-ARs have been reported in mouse and human sperm and have a molecular weight of approximately 72 kDa (Adeoya-Osiguwa et al., 2006). We looked for its presence in rat sperm and, using β-2-AR-specific antibody, detected a distinct band at approximately 72 kDa (Figure 2A). The expression of β-2-AR did not differ between capacitating and non-capacitating sperm.

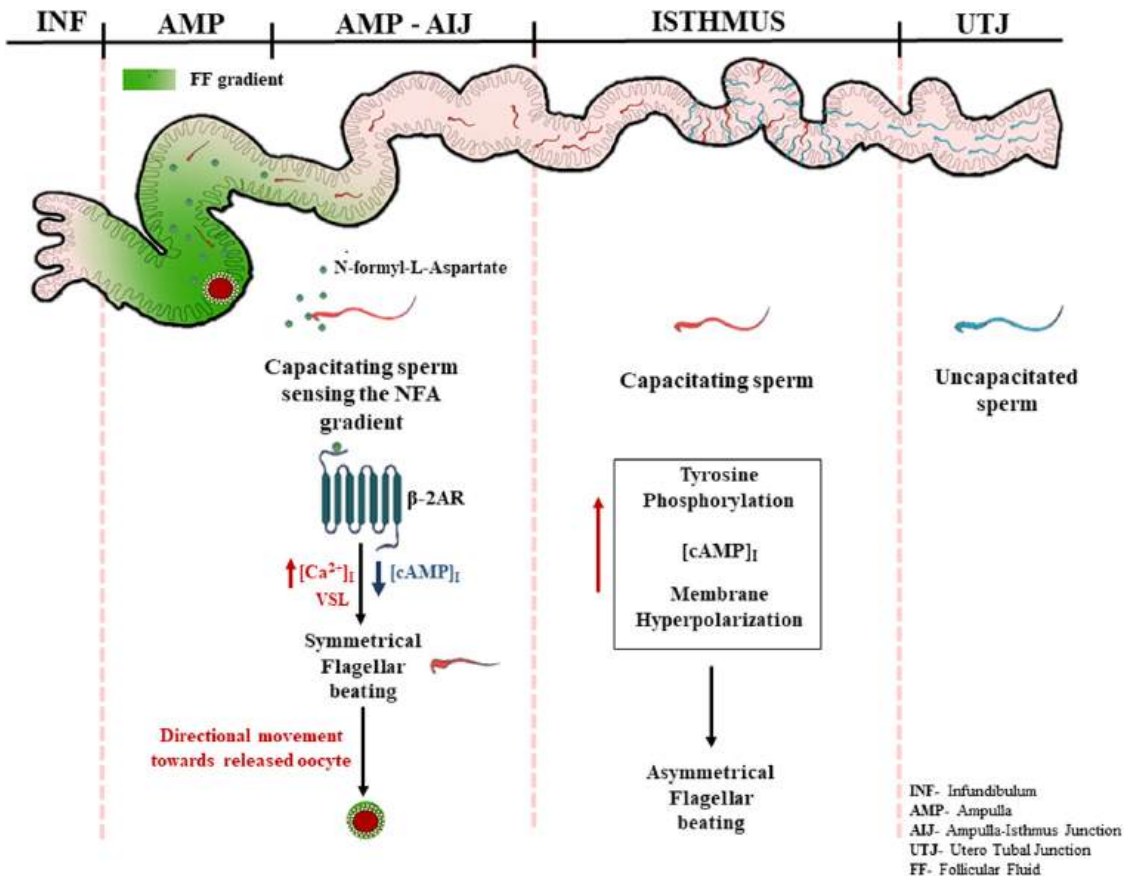

FIGURE 7
Schematic representation for the mechanism of chemotaxis mediated by NFA.

Localization by IIF showed that β-2-ARs are localized on the head and in the mid-piece region of the sperm, with decreasing or fainter fluorescence along the principal piece and end piece. Previously, β-2-ARs have been reported to be localized around the acrosomal cap, head, and neck, along with less intense localization around the tail (Adeoya-Osiguwa et al., 2006). Loss of the positive signal on permeabilization of the sperm membrane indicated its presence on the sperm surface (Figure 2B). This observation suggested that β-2-AR may be the putative receptor for NFA.

To further confirm this possibility, sperm chemotaxis to NFA was determined using ICI-118,551, a β-2-AR specific antagonist. ICI-118,551 is reported to be effective at a concentration of 10 nmol/L in somatic cells (Pecha et al., 2015). We first determined the lowest concentration of the antagonist that was non-toxic to sperm, by checking sperm viability and motility at different concentrations of ICI-118,551 and at time intervals of 15 min from 0–45 min. The effect of ICI-118,551 on sperm motility and viability was found to be in the order 1 μM > 0.1 μM > 0.01 μM with 0.01 M ICI-118,551 showing no detrimental/least detrimental effect on sperm viability (Tables 1, 2). Hence, the chemotactic effect of NFA was tested on sperm pre-treated with 0.01 μM ICI-118,551 for 30 min. A significantly reduced chemotactic response of sperm to NFA affirmed that NFA mediates chemotaxis via the β-2-AR receptors present on sperm (Figure 3).

Ca^{2+} is one of the important ions involved in different sperm processes such as capacitation and acrosome response (Correia et al., 2015). $[Ca^{2+}]_I$ levels have been found to increase during sperm chemotaxis (Teves et al., 2009; Bhagwat et al., 2018). We observed an increase in $[Ca^{2+}]_I$ in capacitating sperm after treatment with 0.01 M NFA. This increase was abrogated in the presence of ICI-118551 (Figures 4A,B). Intriguingly, we observed a significant decrease in $[cAMP]_I$, when capacitating sperm were exposed to 0.01 M NFA for 30 min (**$p < 0.01$; Supplementary Figure S3). However, the intracellular levels of Ca^{2+} were elevated (Figure 4). As per the canonical pathway, β-2-AR signaling occurs through the G_S-adenylyl cyclase–cAMP pathway wherein cAMP increases. It is possible that NFA acts through β-2-AR via the non-canonical pathway. This has been

reportedly seen in HEK-293 cells wherein β-2AR-mediated Ca^{2+} influx has been shown to occur independently of conventional cAMP-dependent signaling (Galaz-Montoya et al., 2017). The elevation of $[Ca^{2+}]_I$ observed by us on exposure of capacitating sperm to NFA may regulate flagellar curvature toward symmetrical beating reported to occur in chemotaxis as opposed to asymmetrical beating that occurs during hyperactivation (Chang and Suarez, 2010).

As capacitation, chemotaxis, and acrosome reaction are tightly associated events, we also investigated whether or not NFA may have a role in these important events. Toward this, we analyzed tyrosine phosphorylation, $[cAMP]_i$ and absolute Em of sperm after treatment with NFA as these parameters are known to be affected during capacitation (Puga Molina et al., 2018). Studies have shown the increased association of tyrosine phosphorylation with hyperactivated motility (Nassar, 1999; Y.-Y. Wang et al., 2021). Our results showed that NFA *per se* did not affect the levels of protein tyrosine phosphorylation (Figures 5A,B). However, with NFA, a slight but significant increase in the $[cAMP]_i$ levels compared to DMEM was noted (Figure 5C). This increase in cAMP is not surprising as on incubation of uncapacitated sperm with NFA for 2.5 h, there is a slight but significant increase in motility compared to that seen in DMEM at 0 h (data not shown). Tyrosine phosphorylation is increased only on capacitation. Hence, we see it with BSA which was used as a positive control of capacitation, but not with NFA in which case it is as much as seen with DMEM, thus providing evidence that NFA does not induce capacitation. Membrane hyperpolarization is also a hallmark of capacitation (Baro Graf et al., 2019). Thus, it can be seen in incubations with BSA (Figure 5D). A slight yet significant depolarization is seen with NFA in comparison to that seen with DMEM, thus affirming that NFA does not induce capacitation. However, the possibility that NFA may inhibit capacitation cannot be ruled out. An acrosome reaction is a prerequisite for successful fertilization. It is well-known that spermatozoa that undergo premature acrosome reactions are unable to recognize a chemoattractant gradient (Guidobaldi et al., 2017) and are unable to fertilize the egg (Barbonetti et al., 2008). The acrosome was not affected by 0.01 M NFA (Figure 6). Taken together, all these observations suggest that 0.01 M NFA may not be involved in capacitation or acrosome reactions.

Based on our knowledge of sperm signaling events from the literature and our own observations, we propose a putative mechanism of chemotaxis mediated by NFA. The high levels of progesterone during ovulation may induce capacitation of the sperm parked within the oviduct, thereby inducing their hyperactivation and release from the sticky milieu of the oviduct following which NFA released into the oviduct during ovulation may direct them toward the oocyte via its interaction with β-2-AR present on the sperm surface, causing an additional increase in the intracellular levels of Ca^{+2}. Increased levels of Ca^{+2} may result in Ca^{+2}-associated symmetrical flagellar beating causing the sperm to move in a linear trajectory with increased velocity toward the egg (Figure 7).

In summary, we report that NFA triggers chemotaxis in sperm and does not induce capacitation or acrosome reactions. NFA mediates its chemotactic effect *via* β-2-AR present on the sperm surface possibly through non-canonical signaling, thereby increasing sperm intracellular calcium levels over and above those seen on capacitation and influencing the linear swimming of the sperm toward the oocyte. This study, thus, ignites the possibility of using NFA as a chemoattractant to select good quality sperm for enhancing the "take home baby" rate of IVF procedures.

Data availability statement

The original contributions presented in the study are included in the article/Supplementary Material; further inquiries can be directed to the corresponding author.

Ethics statement

The studies involving human participants were reviewed and approved by the ICMR-NIRRCH Ethics Committee for Clinical Studies. The patients/participants provided their written informed consent to participate in this study. The animal study was reviewed and approved by the Institutional Animal Ethics Committee (IEAC), National institute for Research in Reproductive and Child Health.

Author contributions

PP conceptualized the study. PP and DP conceived and designed the experiments. DP performed all the experiments and data analysis while SB helped DP with the experiments demonstrating chemotaxis mediated by NFA. PP contributed to the reagents, materials, and analysis tools. PP and DP wrote the manuscript.

Funding

This work was supported by core funding from ICMR-NIRRCH (RA/1265/05-2022).

Acknowledgments

We thank Dr. Venkat Gundabala, Department of Chemical Engineering, and Microfabrication facility at the Centre of Excellence for Nanotechnology (CEN), at IIT-Bombay, for their help in fabrication and bonding of the chemotaxis

device. We also thank the Experimental Animal facility at ICMR-NIRRCH for providing the animals for this study and Madhukar More for his help with animal handling. We thank Shraddha Gandhi and Dipika Shinde from our department, for their assistance with the calcium assay and cAMP ELISA, respectively. We acknowledge with gratitude the financial support provided by ICMR-NIRRCH and the Lady Tata Memorial Trust for providing fellowship to DP.

Conflict of interest

The authors declare that the research was conducted in the absence of any commercial or financial relationships that could be construed as a potential conflict of interest.

Publisher's note

All claims expressed in this article are solely those of the authors and do not necessarily represent those of their affiliated organizations, or those of the publisher, the editors, and the reviewers. Any product that may be evaluated in this article, or claim that may be made by its manufacturer, is not guaranteed or endorsed by the publisher.

Supplementary material

The Supplementary Material for this article can be found online at: https://www.frontiersin.org/articles/10.3389/fcell.2022.959094/full#supplementary-material

References

Adeoya-Osiguwa, S. A., Gibbons, R., and Fraser, L. R. (2006). Identification of functional alpha2- and beta-adrenergic receptors in mammalian spermatozoa. *Hum. Reprod.* 21, 1555–1563. doi:10.1093/humrep/del016

Barbonetti, A., Vassallo, M. R. C., Antonangelo, C., Nuccetelli, V., D'Angeli, A., Pelliccione, F., et al. (2008). RANTES and human sperm fertilizing ability: Effect on acrosome reaction and sperm/oocyte fusion. *Mol. Hum. Reprod.* 14, 387–391. doi:10.1093/molehr/gan031

Baro Graf, C., Ritagliati, C., Stival, C., Balestrini, P. A., Buffone, M. G., and Krapf, D. (2019). Determination of a robust assay for human sperm membrane potential analysis. *Front. Cell Dev. Biol.* 7, 101. doi:10.3389/fcell.2019.00101

Baro Graf, C., Ritagliati, C., Torres-Monserrat, V., Stival, C., Carizza, C., Buffone, M. G., et al. (2020). Membrane potential assessment by fluorimetry as a predictor tool of human sperm fertilizing capacity. *Front. Cell Dev. Biol.* 7, 383. doi:10.3389/fcell.2019.00383

Bhagwat, S., Sontakke, S., Desai, S., Panchal, D., Jadhav, S., and Parte, P. (2021a). N-formyl- l -aspartate: A novel sperm chemoattractant identified in ovulatory phase oviductal fluid using a microfluidic chip. *Andrology* 9, 1214–1226. doi:10.1111/andr.12988

Bhagwat, S., Sontakke, S., Deekshith, K., Parte, P., and Jadhav, S. (2018). Chemotactic behavior of spermatozoa captured using a microfluidic chip. *Biomicrofluidics* 12, 024112. doi:10.1063/1.5023574

Bi, S., Yu, D., Si, G., Luo, C., Li, T., Ouyang, Q., et al. (2013a). Discovery of novel chemoeffectors and rational design of *Escherichia coli* chemoreceptor specificity. *Proc. Natl. Acad. Sci. U. S. A.* 110, 16814–16819. doi:10.1073/pnas.1306811110

Bian, F., Mao, G., Guo, M., Mao, G., Wang, J., Li, J., et al. (2012). Gradients of natriuretic peptide precursor A (NPPA) in oviduct and of natriuretic peptide receptor 1 (NPR1) in spermatozoon are involved in mouse sperm chemotaxis and fertilization. *J. Cell. Physiol.* 227, 2230–2239. doi:10.1002/jcp.22962

Bufe, B., Schumann, T., Kappl, R., Bogeski, I., Kummerow, C., Podgórska, M., et al. (2015a). Recognition of bacterial signal peptides by mammalian formyl peptide receptors: A new mechanism for sensing pathogens. *J. Biol. Chem.* 290, 7369–7387. doi:10.1074/jbc.M114.626747

Burnett, L. A., Anderson, D. M., Rawls, A., Bieber, A. L., and Chandler, D. E. (2011). Mouse sperm exhibit chemotaxis to allurin, a truncated member of the cysteine-rich secretory protein family. *Dev. Biol.* 360, 318–328. doi:10.1016/j.ydbio.2011.09.028

Caballero-Campo, P., Buffone, M. G., Benencia, F., Conejo-García, J. R., Rinaudo, P. F., and Gerton, G. L. (2013). A role for the chemokine receptor CCR6 in mammalian sperm motility and chemotaxis: Chemokines, receptors, and sperm chemotaxis. *J. Cell. Physiol.* 229, 68–78. doi:10.1002/jcp.24418

Chang, H., and Suarez, S. S. (2010). Rethinking the relationship between hyperactivation and chemotaxis in mammalian sperm. *Biol. Reprod.* 83, 507–513. doi:10.1095/biolreprod.109.083113

Correia, J., Michelangeli, F., and Publicover, S. (2015). Regulation and roles of Ca2+ stores in human sperm. *REPRODUCTION* 150, R65–R76. doi:10.1530/REP-15-0102

Eisenbach, M. (1999). Mammalian sperm chemotaxis and its association with capacitation. *Dev. Genet.* 25, 87–94. doi:10.1002/(SICI)1520-6408(1999)25:2<87::AID-DVG2>3.0.CO;2-4

Flegel, C., Vogel, F., Hofreuter, A., Schreiner, B. S. P., Osthold, S., Veitinger, S., et al. (2016). Characterization of the olfactory receptors expressed in human spermatozoa. *Front. Mol. Biosci.* 2, 73. doi:10.3389/fmolb.2015.00073

Frolikova, M., Otcenaskova, T., Valasková, E., Postlerova, P., Stopkova, R., Stopka, P., et al. (2020). The role of taste receptor mTAS1R3 in chemical communication of gametes. *Int. J. Mol. Sci.* 21, 2651. doi:10.3390/ijms21072651

Galaz-Montoya, M., Wright, S. J., Rodriguez, G. J., Lichtarge, O., and Wensel, T. G. (2017). β2-Adrenergic receptor activation mobilizes intracellular calcium via a non-canonical cAMP-independent signaling pathway. *J. Biol. Chem.* 292, 9967–9974. doi:10.1074/jbc.M117.787119

Gnessi, L., Fabbri, A., Silvestroni, L., Moretti, C., Fraioli, F., Pert, C. B., et al. (1986a). Evidence for the presence of specific receptors for NFormyl chemotactic peptides on human spermatozoa. *J. Clin. Endocrinol. Metab.* 63, 841–846. doi:10.1210/jcem-63-4-841

Guidobaldi, H. A., Hirohashi, N., Cubilla, M., Buffone, M. G., and Giojalas, L. C. (2017). An intact acrosome is required for the chemotactic response to progesterone in mouse spermatozoa. *Mol. Reprod. Dev.* 84, 310–315. doi:10.1002/mrd.22782

Guidobaldi, H. A., Teves, M. E., Uñates, D. R., and Giojalas, L. C. (2012). Sperm transport and retention at the fertilization site is orchestrated by a chemical guidance and oviduct movement. *Reproduction* 143, 587–596. doi:10.1530/REP-11-0478

Ijiri, Y., Matsumoto, K., Kamata, R., Nishino, N., Okamura, R., Kambara, T., et al. (1994a). Suppression of polymorphonuclear leucocyte chemotaxis by *Pseudomonas aeruginosa* elastase *in vitro*: A study of the mechanisms and the correlation with ring abscess in pseudomonal keratitis. *Int. J. Exp. Pathol.* 75, 441–451.

Inaba, K. (2003). Molecular architecture of the sperm flagella: Molecules for motility and signaling. *Zool. Sci.* 20, 1043–1056. doi:10.2108/zsj.20.1043

Isobe, T., Minoura, H., Tanaka, K., Shibahara, T., Hayashi, N., and Toyoda, N. (2002). The effect of RANTES on human sperm chemotaxis. *Hum. Reprod.* 17, 1441–1446. doi:10.1093/humrep/17.6.1441

Ko, Y.-J., Maeng, J.-H., Lee, B.-C., Lee, S., Hwang, S. Y., and Ahn, Y. (2012). Separation of progressive motile sperm from mouse semen using on-chip chemotaxis. *Anal. Sci.* 28, 27–32. doi:10.2116/analsci.28.27

Naccache, P. H., Levasseur, S., Lachance, G., Chakravarti, S., Bourgoin, S. G., and McColl, S. R. (2000a). Stimulation of human neutrophils by chemotactic factors is associated with the activation of phosphatidylinositol 3-kinase gamma. *J. Biol. Chem.* 275, 23636–23641. doi:10.1074/jbc.M001780200

Nassar, A., MorshediM.Lin, M. H., Srisombut, C., and Oehninger, S. (1999). Modulation of sperm tail protein tyrosine phosphorylation by pentoxifylline and its correlation with hyperactivated motility. *Fertil. Steril.* 71, 919–923. doi:10.1016/S0015-0282(99)00013-8

Oliveira, R. G., Tomasi, L., Rovasio, R. A., and Giojalas, L. C. (1999). Increased velocity and induction of chemotactic response in mouse spermatozoa by follicular and oviductal fluids. *J. Reprod. Fertil.* 115, 23–27. doi:10.1530/jrf.0.1150023

Pecha, S., Flenner, F., Söhren, K., Lorenz, K., Eschenhagen, T., and Christ, T. (2015). β_1 Adrenoceptor antagonistic effects of the supposedly selective β_2 adrenoceptor antagonist ICI 118, 551 on the positive inotropic effect of adrenaline in murine hearts. *Pharmacol. Res. Perspect.* 3, e00168. doi:10.1002/prp2.168

Puga Molina, L. C., Luque, G. M., Balestrini, P. A., Marín-Briggiler, C. I., Romarowski, A., and Buffone, M. G. (2018). Molecular basis of human sperm capacitation. *Front. Cell Dev. Biol.* 6, 72. doi:10.3389/fcell.2018.00072

Schneider, C. A., Rasband, W. S., and Eliceiri, K. W. (2012). NIH image to ImageJ: 25 years of image analysis. *Nat. Methods* 9, 671–675. doi:10.1038/nmeth.2089

Shiba, K., and Inaba, K. (2022). The roles of two CNG channels in the regulation of ascidian sperm chemotaxis. *Int. J. Mol. Sci.* 23, 1648. doi:10.3390/ijms23031648

Southgate, E. L., He, R. L., Gao, J.-L., Murphy, P. M., Nanamori, M., and Ye, R. D. (2008a). Identification of formyl peptides from *Listeria monocytogenes* and *Staphylococcus aureus* as potent chemoattractants for mouse neutrophils. *J. Immunol.* 181, 1429–1437. doi:10.4049/jimmunol.181.2.1429

Teves, M. E., Barbano, F., Guidobaldi, H. A., Sanchez, R., Miska, W., and Giojalas, L. C. (2006). Progesterone at the picomolar range is a chemoattractant for mammalian spermatozoa. *Fertil. Steril.* 86, 745–749. doi:10.1016/j.fertnstert.2006.02.080

Teves, M. E., Guidobaldi, H. A., Uñates, D. R., Sanchez, R., Miska, W., Publicover, S. J., et al. (2009). Molecular mechanism for human sperm chemotaxis mediated by progesterone. *PLoS ONE* 4, e8211. doi:10.1371/journal.pone.0008211

Wang, Y.-Y., Sun, P.-B., Li, K., Gao, T., Zheng, D.-W., Wu, F.-P., et al. (2021). Protein kinases regulate hyperactivated motility of human sperm. *Chin. Med. J.* 134, 2412–2414. doi:10.1097/CM9.0000000000001551

Yang, D., Zhou, Q., Labroska, V., Qin, S., Darbalaei, S., Wu, Y., et al. (2021). G protein-coupled receptors: Structure- and function-based drug discovery. *Signal Transduct. Target. Ther.* 6, 7. doi:10.1038/s41392-020-00435-w

Zhang, M., Hong, H., Zhou, B., Jin, S., Wang, C., Fu, M., et al. (2006). The expression of atrial natriuretic peptide in the oviduct and its functions in pig spermatozoa. *J. Endocrinol.* 189, 493–507. doi:10.1677/joe.1.06483

Check for updates

Received: 1 June 2020 | Revised: 23 January 2021 | Accepted: 15 February 2021

DOI: 10.1111/andr.12988

ORIGINAL ARTICLE

ANDROLOGY WILEY

N-formyl-L-aspartate: A novel sperm chemoattractant identified in ovulatory phase oviductal fluid using a microfluidic chip

Shweta Bhagwat[1] | **Shraddha Sontakke**[2] | **Sneha Desai**[2] | **Durva Panchal**[2] | **Sameer Jadhav**[1] | **Priyanka Parte**[2]

[1]Department of Chemical Engineering, Indian Institute of Technology Bombay, Powai, Mumbai, India

[2]Department of Gamete Immunobiology, ICMR-National Institute for Research in Reproductive Health, Parel, Mumbai, India

Correspondence
Sameer Jadhav, Department of Chemical Engineering, Indian Institute of Technology Bombay, Powai, Mumbai—400076, India.
Email: srjadhav@iitb.ac.in

and
Priyanka Parte, Department of Gamete Immunobiology, ICMR-National Institute for Research in Reproductive Health, J. M. Street, Parel, Mumbai—400012, India.
Emails: partep@nirrh.res.in, priyankaparte62@gmail.com

Funding information
ICMR-NIRRH, Grant/Award Number: RA/915/05-2020; Department of Biotechnology , Ministry of Science and Technology, Grant/Award Number: # BT/PR13442/MED/32/440/2015

Abstract

Background: Chemotaxis, as a mechanism for sperm guidance although known, has been difficult to demonstrate in vitro. Consequently, very few chemoattractants have been identified till date.

Objectives: To investigate sperm motility behavior in response to ovulatory (OV) and preovulatory (preOV) oviductal fluid (OF) and identify potential chemotactic metabolites.

Materials and Methods: Intracellular calcium ($[Ca^{2+}]_I$) influx in capacitating sperm was determined by spectrofluorimetry. The chemotactic response of rat caudal sperm to OF from the preOV- and OV- phases of normally cycling female rats was assessed in a microfluidic device developed by us. Hydrophilic metabolites extracted from the OF of both the phases were resolved and identified by LC-MS/MS, followed by data analysis using XCMS and MetaboAnalyst software, and chemotactic potential of the most promising compound was validated using the microfluidic device.

Results: Spectrofluorimetric analysis depicts a significant increase in sperm $[Ca^{2+}]_I$ in response to OV-OF. With the microfluidic chemotaxis assay, sperm population shows a significantly increased directionality and velocity to an ascending gradient of 0.06 µg/µl OV-OF compared to preOV-OF. LC-MS/MS of the OFs demonstrates five and four metabolites to be exclusive to the OV-OF and preOV-OF, respectively, and 25 metabolites common to both, of which 14 metabolites, including N-formyl-L-aspartate (NFA), are increased in OV-OF; NFA was tested for its ability to influence sperm movement, and shows chemotaxis potential.

Discussion and Conclusion(s): This is the first study that has systematically demonstrated sperm chemotaxis with OV phase rat OF, identified NFA present in this fluid as a novel chemoattractant to sperm, and proven the utility of the device to test putative chemoattractants. It remains to be seen whether NFA is present in the follicular fluid (FF) of infertile women, and whether it may likely be a reason for the failure of natural conception in idiopathic infertile women.

KEYWORDS
chemoattractants, intracellular calcium influx, LC-MS/MS, metabolomics, sperm chemotaxis

© 2021 American Society of Andrology and European Academy of Andrology

1 | INTRODUCTION

Nature has made its modus operandi fool-proof with a continuous replenishment of highly active and responsive sperm, in small packets, by a process termed as capacitation to achieve fertilization success in vivo.[1,2] Once sperm undergo capacitation, they begin to respond to a concentration gradient of chemoattractant/s, by the mechanism of chemotaxis. It is evident that this mechanism occurs within a very small fraction of responsive cells (2–12%) at a given time, from the total population, as the capacitating sperm population itself is low.[1,3,4] Chemotaxis as a guidance mechanism for directing sperm movement to the oocyte is well established.[5,6] However, while several have been proposed only a few chemoattractants for mammalian sperm have been identified and confirmed so far.[7–13]

At the onset of ovulation, the Cumulus-Oocyte-Complex (COC) is released in the female oviduct/fallopian tube. In humans, both the oocyte and the cumulus cells are known to be a source of these chemical stimulants.[14] Additionally, once the oocyte is released in the oviduct, the oviductal epithelium also secretes chemoattractants. Sperm can sense these attractants and orient their swimming direction toward the oocyte. This phenomenon has been observed in internal as well as external fertilizers. Although there exists differences between physiological adaptations of the sperm in both of the aforementioned cases, the two share common origins of their respective chemoattractants. Natriuretic peptide type C (NPPC) in the mouse[9] and allurin in *Xenopus laevis*[10] have their origin from the oviductal epithelium. Follicular and oviductal fluids (OFs) have also been evaluated for inducing chemotaxis in sperm.[9,15–18] Thus, the process of ovulation triggers the release of certain compounds in the OF, which could serve as a cohort of such stimulants. Progesterone, a steroid hormone, which is secreted by the cumulus cells, is one such chemoattractant studied extensively across species.[8,19] Interestingly, in rabbits, progesterone is secreted only by the cumulus cells and not by the oocyte.[20] Apart from this, there is very little information on the identity of any other chemoattractant/s coming from the follicular fluid; although some compounds have been identified, their role in sperm chemotaxis has not been demonstrated. One study suggested that the oocyte-derived chemoattractant is a hydrophobic non-peptide molecule, which is associated with a carrier protein that keeps it intact even in a hydrophilic environment.[21] This molecule has its chemotactic ability intact in hexane-extracted hydrophobic fraction of oocyte-conditioned medium as well as in the aqueous phase; however, the identity of this molecule is yet unknown.

Several approaches have been tried by different groups for the identification of novel chemoattractants in the follicular fluid (FF). Initially, to identify these chemoattractants present in the FF, its components were tested for the induction of sperm chemotaxis.[22–25] This was the fastest possible approach; however, the conventional capillary assay used could not differentiate chemotaxis from other means of sperm accumulation.[7] Serrano et al., followed a top-down approach, where they fractionated the FF and found that the chemotactic activity in the active fraction could be associated with an 8.6 kDa protein.[17] By N-terminal sequencing, they obtained the sequence of this protein, and found it to be closely related to Apolipoprotein B2, toward the N-terminal end. These studies suggested that chemoattractants are most likely small proteins or molecules.

It is well known that these attractants can induce sperm chemotaxis only if a stable concentration gradient is established that required the presence of a controlled chemical environment, easily feasible in vitro using microfluidics.[12] In vivo, a spatial gradient forms with higher concentrations closer to the egg, and lower concentrations away from it.[7] Most of the mammalian chemotaxis studies have suggested that the gradient formed in the oviduct is limited over shorter distances due to the presence of oviductal contractions and fluid flow.[26] However, the presence of the chemoattractant, natriuretic peptide precursor A (NPPA), in the mouse oviduct from ampulla to the uterotubal junction[27] predicts the possibility of a longer range for chemotaxis, in vivo.[26] In a recent study, the existence of any sperm guidance mechanism in the mouse oviduct was challenged, wherein sperm oocyte interaction and successful fertilization was demonstrated attributing it to adovarian peristalsis, uninterrupted OF flow and sperm's inherent motility.[28] However, several questions still remain unanswered.

The present work focused on sperm motility behavior in response to ovulatory (OV) and preovulatory (preOV) phase OF. Having observed remarkable differences, we went on to identify the factors released on ovulation that may likely induce a chemotactic response in sperm. In this context, metabolites were the most appropriate target molecules. These, being small in size, diffuse faster and therefore the possibility of them forming a gradient within a short time in the oviductal lumen is high. Hence, we determined the metabolomic differences in OV- vis-à-vis preOV-OF in an attempt to identify the chemoattractant/s.

2 | MATERIALS AND METHODS

Adult male and female rats housed in four per cage and maintained under conditions of 14 h light and 10 h dark at the ICMR-NIRRH Animal Facility were used. Food and water were provided ad libitum. All experiments were performed in compliance with the CPCSEA guidelines and approval of the Institutional Animal Ethics Committee of the Indian Council for Medical Research-National Institute for Research in Reproductive Health (ICMR-NIRRH), Mumbai. This study was approved by the Scientific Advisory Committee of ICMR-NIRRH.

2.1 | Isolation of oviductal fluid (OF)

Three-month-old Holtzman inbred female rats were sacrificed by CO_2 asphyxiation in their OV- and preOV- phases classified by assessing the vaginal lavage of the female rats collected between 09:00 am and 11:00 am, under an upright light microscope (10× magnification, Carl Zeiss Microscope).[29] The OF was collected either in Dulbecco's minimum essential medium (DMEM; Thermo Fischer

20472927, 2021, 4, Downloaded from https://onlinelibrary.wiley.com/doi/10.1111/andr.12988 by Icmr - National Institute For Research In Reproductive And Child Health, Wiley Online Library on [27/08/2024]. See the Terms and Conditions (https://onlinelibrary.wiley.com/terms-and-conditions) on Wiley Online Library for rules of use; OA articles are governed by the applicable Creative Commons License

Scientific) for microfluidic assays,[12] or in LC-grade water for OV- and preOV- OF-mediated calcium influx studies and metabolomic studies. The OF samples collected in DMEM were centrifuged at 2000 ***g*** for 5 min at 4°C and snap-frozen in liquid nitrogen, whereas the ones collected in water were aliquoted after centrifugation, snap-frozen, and lyophilized to prevent degradation of metabolites over time. All the samples were stored at −80°C until use.

2.2 | Preparation of spermatozoa

Spermatozoa (sperm) were isolated from the cauda epididymis of sexually mature 3-month-old Holtzman inbred male rats and were maintained under capacitating conditions as described earlier.[12] Sperm motility was determined immediately on preparation of sperm sample, at 2.5 h in capacitation medium, and at the end of the chemotaxis assay (<5.5 h) as described earlier,[12] to ensure that sperm motility remained >70%[30] till the end of the experiment.

2.3 | Measurement of $[Ca^{2+}]_I$ concentration in sperm

Fura-2AM dye (Sigma Aldrich, MO, USA) was used to determine the $[Ca^{2+}]_I$ concentration in capacitating rat caudal sperm using a published protocol.[31,32] Briefly, 10^7 capacitating rat sperm were incubated with 5 µM Fura-2AM (dissolved in DMSO with 0.05% F-127 Pluronic; final concentration of DMSO 0.1%) at 37°C for 45 min in DMEM, with intermittent mixing. The dye-loaded cells were washed three times in DMEM by centrifugation and resuspended in Ca^{2+} containing Tyrode's buffer. 2×10^6 capacitating sperm were then added to different concentrations of OV-OF, maintaining the final volume to 200 µl. Buffer control consisted of 2×10^6 capacitating sperm resuspended in calcium containing Tyrode's buffer. For assessing OV- versus preOV-OF-mediated calcium influx, 10^7 capacitating sperm were used for the assay. Sperm were evenly resuspended by mixing for 30 s in the orbital shaker inbuilt in the spectrofluorimeter. Fura-2AM excitation was set at 340 nm and 380 nm to determine the bound and free calcium, respectively, with an emission at 500 nm in the spectrofluorimeter (µQuant, BioTek Instruments Inc.). Fluorescence readings were recorded at an interval of 13–14 s, for 10–15 min. Cells were then lysed with 1% Triton X-100 followed by addition of 3 mM $CaCl_2$ for F_{max} and 2 mM $MnCl_2$ for F_{min}.[32] The concentration of Ca^{2+} was calculated using the equation $[Ca^{2+}]_I = K_d^*[(F - F_{min})/(F_{max} - F)]$, where K_d (224 nM) is the dissociation constant of the dye at 37°C, F is the fluorescence reading of sample which is the ratio of F_{340} to F_{380}, and F_{max} and F_{min} are the respective maximum and minimum calcium levels over 5 min in the milieu. Before testing the response of OV- and preOV- OF, a basal fluorescence reading was obtained at a concentration of 10^7 cells/200 µl. Later this basal reading was subtracted from the reading obtained for OV- and preOV- OF, in order to reduce well-to-well variation and the corresponding $[Ca^{2+}]_I$ was normalized to its buffer control. All datasets were analyzed using Prism 8.4.0 software (GraphPad Software, Inc.). Differences between the two groups were analyzed using unpaired Student's *t*-test and were considered statistically significant when *p*-value was less than or equal to 0.05.

2.4 | Microfluidic device fabrication and chemotaxis assays

The micropattern from the silicon master[12] was transferred on to a polydimethylsiloxane (PDMS) slab using the silicone elastomer kit (Sylgard® 184, Dow Corning Corp.) and the microfluidic device was fabricated as described earlier.[12]

The device was prepared and set-up for the chemotaxis assay.[12] Capacitated sperm were added to the cell reservoir, and the microfluidic chip was placed on the microscope stage, enclosed in a chamber maintained at 37°C. A concentration gradient of the fluid to be tested was allowed to form in the transverse channel by aspirating fluid at a rate of 1 µL/min with a syringe pump (NE-1000, New Era Pump Systems Inc.). The flow and gradient were allowed to stabilize for 10 min, after which sperm motion in the transverse channels was recorded at 10X magnification using the sCMOS camera to capture 2058x512 square pixel, 8-bit MPTIFF images at 91 fps for 15 s. Each experimental run was carried out for <1 h to record ~30 such movies of 15 s duration, and a maximum of three runs were carried out for each biological replicate.

2.5 | Design of experiments for the chemotaxis assay with OF

For these experiments, 12 independent OF samples were used with protein concentration maintained at 0.06 µg/µl for each experiment. Six female rats in their OV- and eight in the preOV- phase were sacrificed. In case of preOV-OF, two samples each comprised of fluid pooled from at least four oviducts of two female rats.

Six male rats were used to obtain sperm samples for experiments related to chemotactic response to OV- and preOV- OF along with the DMEM control ($n = 6$). After incubating sperm under capacitating conditions for 2.5 h, they were exposed to three conditions; media (M), gradients of OV- (O), and preOV- (P) fluid for each experimental run. To account for variability in the time of exposure for each experimental run, the sequence of exposure was shuffled (MPO, POM, OMP, MOP, OPM, PMO). The sperm population size analyzed for each experimental condition was $n \geq 469$.

2.6 | Estimation of chemotaxis and statistical analysis

We determined sperm chemotaxis by assessing their swimming bias in the direction of the gradient generated with 0.06 µg/µl of preOV- and OV- phase OFs. This was done by calculating the combined odds ratio for sperm directionality in the abovementioned conditions. For

20472927, 2021, 4, Downloaded from https://onlinelibrary.wiley.com/doi/10.1111/andr.12988 by Icmr - National Institute For Research In Reproductive And Child Health, Wiley Online Library on [27/08/2024]. See the Terms and Conditions (https://onlinelibrary.wiley.com/terms-and-conditions) on Wiley Online Library for rules of use; OA articles are governed by the applicable Creative Commons License

each condition, the total number of sperm swimming in left-to-right (L-R) and right-to-left (R-L) directions, respectively, in the transverse channel (test zone of the device) was determined from the above six experiments. A combined odds parameter (combined $Odds_{gradient}$) was calculated by taking a ratio of the number of cells moving toward the gradient direction (L-R, ascending) to those moving in the opposite direction (R-L, descending). A similar odds parameter was also calculated for media control (combined $Odds_{media}$ = L-R/R-L). The chemotactic response was revealed in the combined odds ratio (O.R.) where each of the gradient conditions was normalized with its respective control (combined O.R. = combined $Odds_{gradient}$/combined $Odds_{media}$).[21] Thus, O.R.s of OV- and preOV- OF were compared using media control as a baseline.[33] In addition to this, we also calculated a combined O.R. of OV- and preOV- gradient to test sperm biased motion toward either of the gradients. The combined O.R. values are expected to be close to 1 if the swimming was random; and >1 when the swimming was biased in the gradient direction.[21,34] To account for variability in the experimental runs, the standard error was calculated using the logit method described elsewhere,[33] that uses normal approximation to the distribution of the logarithm of the odds ratio.

Secondly, for the quantification of chemotaxis, we determined whether sperm had a preferential bias in its speed toward a chemoattractant and calculated the net distance "d" traveled by a sperm in the transverse channel,[16,18] normalized with the time of travel. This, by definition, is the sperm straight-line velocity (VSL) which was determined for sperm moving from left to right and for those moving from right to left, in the transverse channels. The net distance "d" was calculated using: $d = \sqrt{(x_2 - x_1)^2 + (y_2 - y_1)^2}$ where (x_1, y_1) and (x_2, y_2) are the *x* and *y* coordinates of the initial and final positions of the sperm head, obtained using manual tracking plugin in ImageJ software (ver.1.50b, NIH, USA).[35] Thirdly, percentage frequency distribution of the VSL was plotted for all the conditions tested, to check for the percentage of chemotactic population.

All datasets were analyzed using Prism 8.4.0 software (GraphPad Software, Inc.). Normality test for velocity distribution of sperm populations was carried out using Shapiro-Wilk test. Since the VSL values showed a non-normal distribution, a non-parametric ANOVA (Kruskal-Wallis test) was used with Dunn's post-test for multiple comparisons. The combined O.R. was analyzed for statistical significance using the Chi-squared test, where 99% confidence interval and *p*-value for each combined O.R. were calculated. Differences were considered statistically significant when *p*-value was less than or equal to 0.05.

2.7 | Metabolite extraction

Three individual samples of the lyophilized OV- and preOV- OF were reconstituted in LC-grade water and 20 µg of each was pooled for OV- and preOV- group, respectively. To this pool, five volumes of cold (−20°C) chloroform-methanol (2:1 vol/vol)[36] solution were added, vortexed, and incubated overnight at 4°C. The upper aqueous fraction containing hydrophilic metabolites was collected by centrifugation at 12,000 ***g*** for 10 min at 4°C, was vacuum dried, and stored at −80°C until use. Samples were reconstituted in 20 µl LC-grade water prior to loading on the column.

2.8 | Metabolite separation using LC-MS/MS

Three microliters of resuspended aqueous phase sample extracts for OV- and preOV- OF were separated by Reverse Phase chromatography in triplicates. For normalization, each sample was spiked with 1 ppm reserpine (Sigma-Aldrich), which served as an internal standard. Hydrophilic metabolite separation was performed using Hypersil Gold HILIC (100 × 2.1 mm × 3 µm, Thermo Fisher Scientific), on an Agilent 1290 Infinity UHPLC system (Agilent Technologies), run at a flow rate of 0.3 µl/min, and controlled by MassHunter™ Acquisition software (Agilent Technologies). Mobile phase A was 0.1% formic acid in water, whereas mobile phase B was 0.1% formic acid in 90% ACN:10% water. The separated metabolites were then analyzed on Agilent 6550 iFunnel Quadrupole Time-of-Flight LC/MS (Q-TOF) equipped with an electrospray (ESI) ion source (Agilent Technologies). LC/MS was performed in the positive ion mode. Full MS scans were acquired from m/z 60–1000, at a scan rate of 1 spectra/s.

2.9 | LC-MS/MS data acquisition

Untargeted data acquisition was performed using LC/Q-TOF in the MS/MS mode and data obtained were deconvoluted into individual chemical peaks with Agilent MassHunter™ Qualitative Analysis B.06.00 (MassHunter™ Qual; Agilent Technologies).[37] Every data file was extracted as ".d" formatted file and was used for subsequent statistical analysis and data visualization in XCMS ONLINE software.

2.10 | LC-MS/MS data analysis using XCMS ONLINE

The raw data files (.d) obtained after data acquisition were converted to.mzML format using the ProteoWizard MSConvert tool.[38] The.mzML file of each of the OV- and preOV- OF replicates was then uploaded to a single dataset on XCMS ONLINE.[39–41] Pair-wise analysis job was created and OV- versus preOV- datasets were analyzed. The predefined parameter set for HPLC/Q-TOF instrument was used with a fold change set to 1.5 and *p*-value ≤0.01.

2.11 | LC-MS/MS data analysis using MetaboAnalyst

The data obtained from XCMS were arranged in the file format specified for "MS Peaks to Pathways" in the MetaboAnalyst software.[42] Metabolites increased or decreased in the OV-OF were listed in separate files, for proper bifurcation of the origin of the metabolite. Data for pathway analysis were loaded in the "MS Peaks to Pathways" in the software and

20472927, 2021, 4, Downloaded from https://onlinelibrary.wiley.com/doi/10.1111/andr.12988 by Icmr - National Institute For Research In Reproductive And Child Health, Wiley Online Library on [27/08/2024]. See the Terms and Conditions (https://onlinelibrary.wiley.com/terms-and-conditions) on Wiley Online Library for rules of use; OA articles are governed by the applicable Creative Commons License

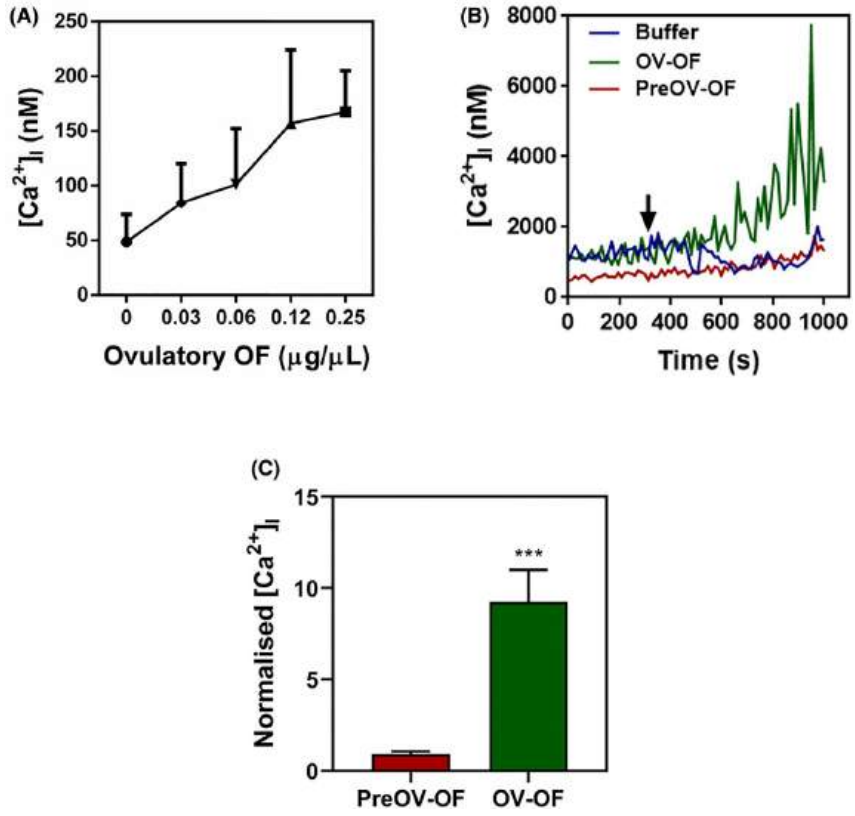

FIGURE 1 Intracellular calcium $[Ca^{2+}]_I$ influx in OF-stimulated capacitating spermatozoa. Sperm $[Ca^{2+}]_I$ was assessed on exposure to 0, 0.03, 0.06, 0.12, and 0.25 µg/µL OV-OF (n = 3 biological replicates), where a typical ratiometric increase was observed (A). A representative graph for $[Ca^{2+}]_I$ influx induced with 0.06 µg/µl of OV- and preOV- OF (indicated with an arrow at 314 s) in sperm (B). Normalized $[Ca^{2+}]_I$ in response to 0.06 µg/µl of OV- and preOV- OF (n ≥ 3 biological replicates) (C). Values are expressed as mean ±SEM. Fura-2AM-loaded capacitating sperm were stimulated with OV- or preOV- OF and the corresponding F_{max} and F_{min} values were recorded after addition of 1% Triton X-100. Excitation of the dye with calcium bound and unbound was carried out at 340 and 380 nm, respectively, and fluorescence emission measured at 500 nm. $[Ca^{2+}]_I$ was calculated as described in "Materials and Methods". Sperm responded with increased $[Ca^{2+}]_I$ toward 0.06 µg/µL of OV-OF as compared to preOV-OF at the same concentration. "***": $p < 0.0005$

subjected to analysis with a mass accuracy of 5 ppm. Mummichog algorithm was selected for enrichment analysis with a p-value cut-off of 0.001. Pathway library for *Rattus Norvegicus* (Rat species) was selected, which was linked to the KEGG database. Metabolites and their biologically relevant pathways were identified using the KEGG database.

2.12 | Statistical analysis for metabolomics

Clustering analysis was done using XCMS software, to get the comparative heat-map of the technical replicates for the two groups. Using univariate statistical analysis, fold change and p-value were plotted together in the cloud plot in XCMS for increased and decreased metabolites in the two groups. Multivariate statistical analysis was carried out using principal component analysis (PCA) in the MetaboAnalyst software, in order to discern if there was a difference in the metabolomic profile between OV- and preOV- OF.

The metabolites that showed significant statistical differences between OV- and preOV- OF were studied further. A literature review was performed using PubMed to identify relevant articles based on search terms such as "metabolite name and its role in chemotaxis". Active clinical trials/patents were also reviewed using PubChem search for the metabolite identified.

3 | RESULTS

3.1 | OV-phase OF triggers $[Ca^{2+}]_I$ in sperm

In order to ensure whether OV-OF induced an $[Ca^{2+}]_I$ influx in capacitating sperm, Fura-2AM-loaded sperm were directly resuspended in OV-OF at protein concentrations of 0.03, 0.06, 0.12, and 0.25 µg/µl, and fluorescence intensity ratio (F_{340}/F_{380}) was calculated for determining the levels of $[Ca^{2+}]_I$, as described in "Materials and Methods" section. A modest dose-dependent increase in the $[Ca^{2+}]_I$ was observed with OV-OF (Figure 1A). The $[Ca^{2+}]_I$ profile was marked with an immediate increase in the $[Ca^{2+}]_I$ up to 0.12 µg/µl which attained a sustained equilibrium at 0.25 µg/µl OV-OF concentration (Figure 1A). When sperm were exposed to OV-OF at 0.06 µg/µl, we could see a rise in $[Ca^{2+}]_I$ with time (Figure 1B) and was significantly

20472927, 2021, 4, Downloaded from https://onlinelibrary.wiley.com/doi/10.1111/andr.12988 by Icmr - National Institute For Research In Reproductive And Child Health, Wiley Online Library on [27/08/2024]. See the Terms and Conditions (https://onlinelibrary.wiley.com/terms-and-conditions) on Wiley Online Library for rules of use; OA articles are governed by the applicable Creative Commons License

higher (Figure 1C) as compared to buffer control and preOV-OF at the same concentration. Furthermore, sperm $[Ca^{2+}]_I$ in response to preOV-OF were similar to that in buffer control (Figure 1B).

3.2 | Sperm respond chemotactically to OV- OF

The microfluidic device[12] was designed such that sperm have an equal opportunity to enter the transverse channel from either sides of the test zone (Figure 2A). Thus, in order to examine whether the presence of an ascending (left to right) or descending (right to left) OF concentration gradient affected sperm numbers entering the transverse channels (Figure 2A), we calculated the combined O.R. for sperm entering the transverse channels in increasing and decreasing concentration gradient of OV- and preOV- OF. This value was significantly higher than the expected value of 1, for sperm moving in an ascending gradient of OV-OF indicating that sperm exhibited a preferential biased movement toward increasing concentration of OV-OF (Figure 2B). In addition to this, combined O.R. for OV:preOV gradient was significantly higher than unity, suggesting that sperm exhibited chemotactic response toward OV-OF as opposed to preOV-OF. The absolute numbers of sperm moving left to right and right to left are presented in Table S1. In case of sperm exposed to an increasing concentration gradient of preOV-OF, the combined O.R. was very close to the expected value, and hence was statistically insignificant (Figure 2B). A significant increase was observed in mean VSL (Figure 2C) for sperm population moving along an increasing gradient concentration of OV-OF (0.06 μg/μL), as compared to those moving in an increasing gradient of preOV-OF and media control. Also, the mean VSL for sperm moving along increasing gradient of preOV-OF was significantly lower ($p < 0.05$) as compared to that observed for sperm swimming in media alone (Figure 2C).

The frequency distribution curve for OV-OF showed that sperm population exposed to an increasing gradient had relatively higher percentages of sperm in VSL range 40–80 and 80–120 μm/s and lower percentage in VSL range of 0–40 μm/s as compared to other conditions (Figure 2D). We also observed that percentages of sperm in the low VSL range of 0–40 μm/s are higher in case of preOV-OF gradient as compared to the media control.

3.3 | OV-OF shows metabolomic differences with respect to preOV-OF

In order to determine the chemoattractants present in the OV-OF, hydrophilic metabolite fractions of OV- and preOV- OF were

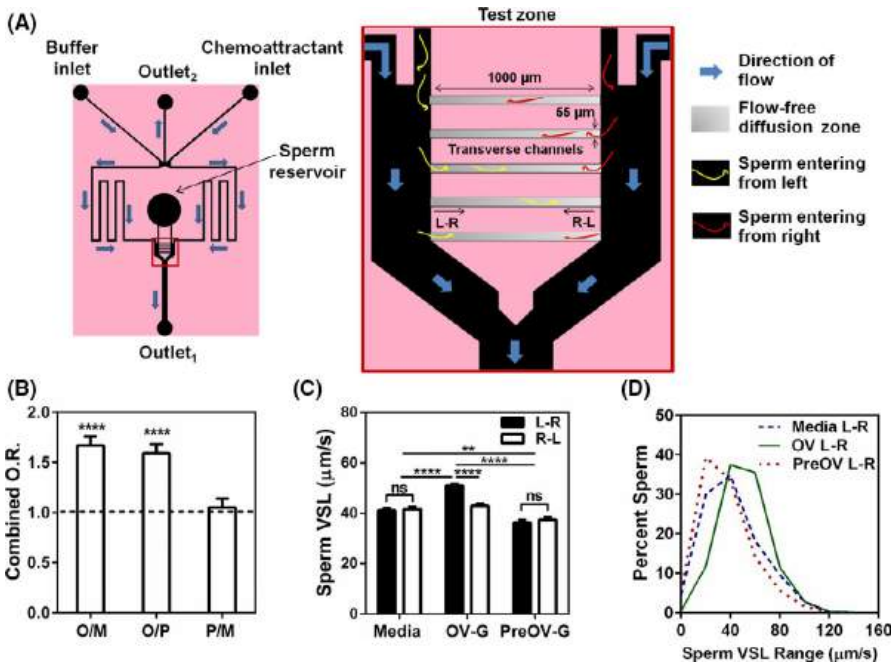

FIGURE 2 Sperm chemotactic response to a concentration gradient of OV- and preOV- OF. Schematic illustration of the flow-profile (blue arrows) in the microfluidic device with an enlarged view of the test zone; wherein sperm (drawn, not to scale) entering the transverse channel from left to right (L-R; increasing concentration gradient) and right to left (R-L; decreasing concentration gradient) are color-coded in yellow and red, respectively (A); Sperm directionality represented by combined odds ratio (O.R.) for the cumulative number of sperm entering the transverse channel for OV-gradient versus media control (O/M), OV- versus preOV- gradient (O/P), and preOV-gradient versus media control (P/M) (B); sperm VSL in response to an increasing (L-R) as well as decreasing (R-L) concentration gradient for different conditions tested (C); and distribution profile of sperm VSL in an ascending (L-R) gradient (D). Sperm exposed to media (M) devoid of OF served as the control. Results are cumulative from six experiments in total. Each column represents average values (± SEM) for individual conditions tested. Sperm VSLs are significantly higher when sperm move along increasing concentration gradient of OV-OF as compared to others. "**": $p < 0.005$, "****": $p < 0.00005$

20472927, 2021, 4, Downloaded from https://onlinelibrary.wiley.com/doi/10.1111/andr.12988 by Icmr - National Institute For Research In Reproductive And Child Health, Wiley Online Library on [27/08/2024]. See the Terms and Conditions (https://onlinelibrary.wiley.com/terms-and-conditions) on Wiley Online Library for rules of use; OA articles are governed by the applicable Creative Commons License

subjected to LC-MS/MS. The data files were extracted into ion chromatograms, with peak matching, retention time correction, and similar peaks aligned.[43] The Total Ion Chromatogram (TIC) illustrates the intensity profile of OV- and preOV- OF mass spectrum. The spectral peaks were clean and well separated from the baseline, such that we could get noise-free peaks (Figure 3A). Reserpine, that was used as an internal standard, was detected in all the samples adding up to the quality control of the LC runs.

Multivariate statistical analysis using the PCA method showed close clustering of individual groups together, further highlighting

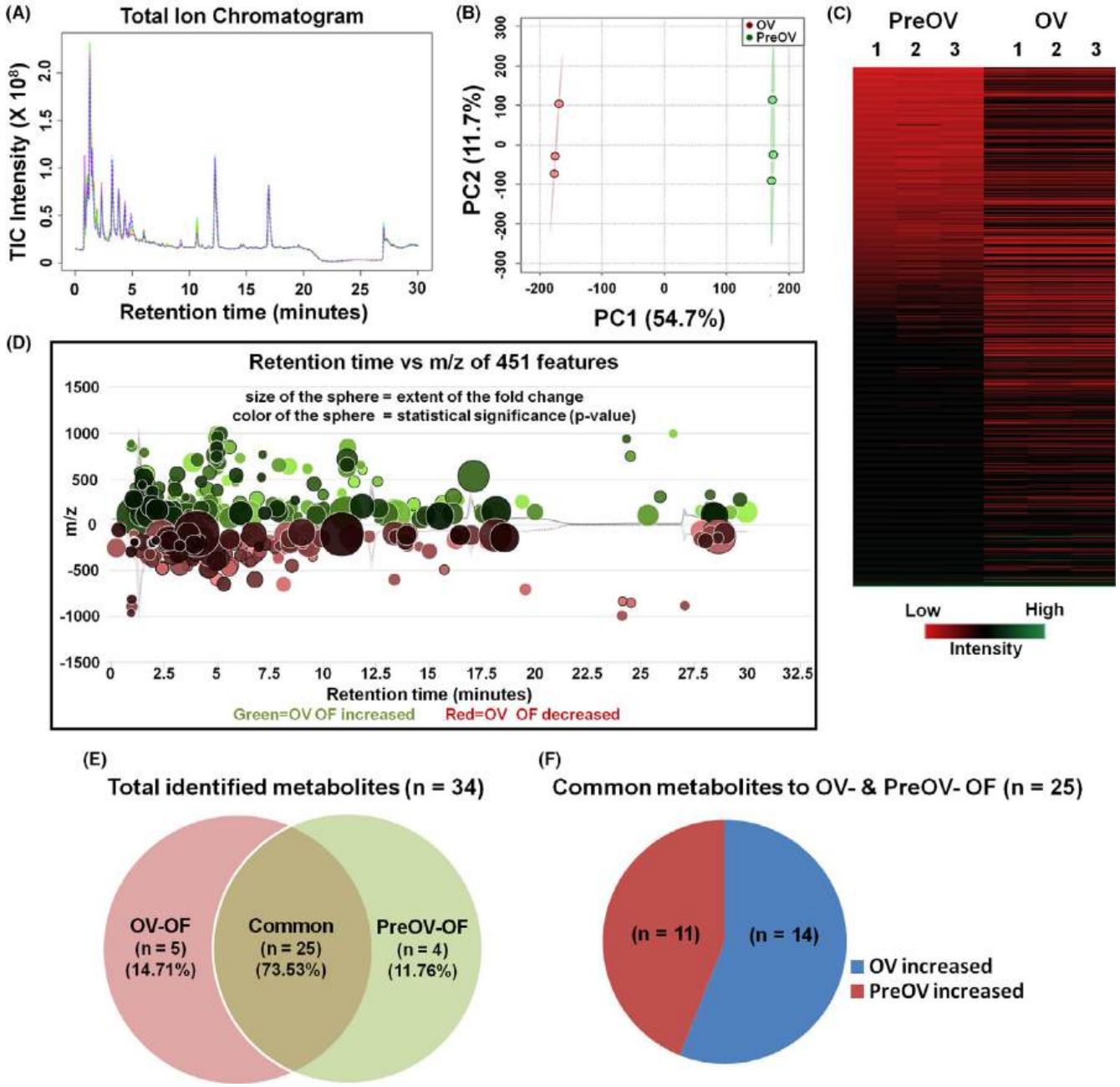

FIGURE 3 Metabolic differences observed by untargeted LC-MS/MS for ovulatory- (OV) and preovulatory (preOV) phase oviductal fluid (OF). Hydrophilic metabolites were extracted using the MPLEx protocol, from OV- and preOV- OF, pooled from three animals in their respective phases of Estrous cycle and subjected to LS-MS/MS analysis in triplicates. Total Ion Chromatogram (TIC) of all samples subjected to LC-MS/MS in positive ion mode (A). Principal Component Analysis (PCA) score plot for OV- and preOV- OF run in triplicates (each technical replicate is represented with a filled circle; red: OV- and green: PreOV- OF) with variances for PC 1 and 2 shown in brackets (B); Heat-map, highlighting the total metabolomic differences between OV- and preOV- OF, with color-coded intensity for increased and decreased metabolites (C); and cloud plot generated in XCMS with $p \leq 0.001$ and fold change≥3 (D); Venn diagram plotted for metabolites identified in XCMS and MetaboAnalyst software with the number of identities exclusive to OV- and preOV- OF as well as common to both the groups (E, F).

20472927, 2021, 4, Downloaded from https://onlinelibrary.wiley.com/doi/10.1111/andr.12988 by Icmr - National Institute For Research In Reproductive And Child Health, Wiley Online Library on [27/08/2024]. See the Terms and Conditions (https://onlinelibrary.wiley.com/terms-and-conditions) on Wiley Online Library for rules of use; OA articles are governed by the applicable Creative Commons License

the data quality. In addition to this, the two groups were distinctly separated from each other, depicting good metabolomic differences (Figure 3B). The heat-map reflected gross differences in the intensities of individual metabolites between the two groups. By and large, the technical replicates were consistent (Figure 3C). Using univariate statistical analysis in XCMS, we obtained the cloud plot highlighting the statistical significance and fold increase and decrease in metabolites in the OV-OF. A total of 3037 features were detected under positive ion mode, of which 451 features were finally shortlisted using p-value cut-off 0.001 and a threefold change (Figure 3D).

Of the 451 features, each feature was manually screened, and noisy peaks were discarded using the XCMS software. These features were filtered based on the number of features that were found in at least two of the three technical replicates. Metabolite identities were displayed with their METLIN ID and the ppm error in their identification, in the software online. An error of 10 ppm was considered as a cut-off, where any identity above that was considered false. The entire data were later subjected to analysis in the MetaboAnalyst: MS Peak to Pathway. A total of 34 metabolites were finally identified using both XCMS and MetaboAnalyst software. From these, five metabolites were found to be exclusive to the OV-OF group (Table 1), whereas four were exclusive to preOV-OF, with a list of 25 metabolites common to both (Figure 3E,F). From these common, 14 metabolites were found to be increased (Table 2), and 11 were decreased in OV-OF. From this list, we selected a metabolite, n-formyl-L-aspartate (NFA; Figure S1), for testing its role in sperm chemotaxis, using the microfluidic device. This metabolite showed the highest significant difference between the two groups (i.e. lowest p-value obtained and was found to be increased in OV-OF (Table 2)).

TABLE 1 Metabolites exclusive to Ovulatory phase oviductal fluid (OV-OF)

Metabolites exclusive to OV-OF	m/z	RT	Fold change	*P*-value
Asp Lys Pro Arg	515.293	1.5533	8.689800137	5.9E-06
Lys Met Met Met	540.233	5.89068	5.636228995	2.1E-05
Tetrahydrocolumbamine	342.173	1.67557	5.264125845	4.9E-05
2-aminomuconate 6-semialdehyde	164.032	1.62635	6.010345062	0.00051
Ile Met Val Trp	548.292	1.62057	9.454873789	0.00086
Key				
XCMS and MetaboAnalyst				
Only XCMS				
Only MetaboAnalyst				

TABLE 2 Metabolites increased in Ovulatory phase oviductal fluid(OV-OF)

Metabolites increased in OV-OF	m/z	RT	Fold change	*P*-value
N-formyl-L-aspartate	162.04033	1.6545	7.693719108	4.436E-06
Oxitropium	332.18574	1.3236333	3.267699566	0.0001109
Phalaenopsine T	362.19342	1.3296833	3.609138201	0.000123
Cytometrinil	186.06613	10.029775	3.876981388	0.0001247
Cinitapride	403.23702	2.2694333	4.359072467	0.0001645
Asp His Ile Trp	570.26578	4.6592167	5.43124652	0.0001867
2-N-Cyclohexyl-1-N-(6-methoxyquinolin-8-yl) butane-1,2-diamine	328.23732	9.9930833	3.823400981	0.0002346
Ala Met Arg Val	476.26614	1.4608833	5.547299903	0.000293
N-Acetyl-D-glucosamine/ N-Acetyl-D-mannosamine	194.10231	1.83665	3.45151925	0.0004092
Leonurine	312.15653	2.93205	2.39157391	0.0004197
Stearoyl-CoA	950.42621	4.9815333	9.752415101	0.0004626
L-Gluconate	180.03834	2.63215	1.572153818	0.0009211
Acetoacetyl CoA	834.13215	4.9732583	3.960473125	0.0009386
Cortisone/aldosterone	361.20005	1.9495917	4.028196058	0.0014329
Key				
XCMS and MetaboAnalyst				
Only XCMS				
Only MetaboAnalyst				

20472927, 2021, 4, Downloaded from https://onlinelibrary.wiley.com/doi/10.1111/andr.12988 by Icmr - National Institute For Research In Reproductive And Child Health, Wiley Online Library on [27/08/2024]. See the Terms and Conditions (https://onlinelibrary.wiley.com/terms-and-conditions) on Wiley Online Library for rules of use; OA articles are governed by the applicable Creative Commons License

3.4 | Sperm respond chemotactically to N-formyl-L-aspartate (NFA)

N-formyl-L-aspartate (NFA) was first tested to determine its toxicity to sperm. This was done by assessing its effect on sperm viability and motility. Sperm viability and motility were assessed at 15, 45, and 75 min of incubation of capacitated caudal sperm without or with 0.01 and 0.001 M NFA. Sperm viability across all the time points for both the concentrations of NFA was comparable (>85%) and did not show any significant difference when compared with the media as well as with each other (Figure S2). At 0.1 M concentration, NFA was insoluble, hence could not be used. Motility was observed to be maintained above 70% for 75 min after capacitation, with both 0.01 and 0.001 M NFA (Figure 4A). Interestingly, enhanced motility was observed with NFA at both the concentrations, as compared to sperm incubated with media alone. Motility in 0.01 M NFA was distinctly higher throughout the incubation as compared to its respective media control, over a period of 75 min. However, it was not statistically significant (Figure 4A).

To discern whether NFA induces chemotaxis in sperm and if it did, whether the sperm response to NFA was exclusively due to chemotaxis, or was it a combined effect of chemotaxis and chemokinesis, sperm were exposed to either gradient (G) or non-gradient (N) concentration of NFA, and their responses were compared to that of sperm exposed to DMEM alone (M; control). Experiments were conducted for G, N, and M, in sets of three in the following sequence, that is, GNM, MGN, and NMG using sperm from individual rats per set. For these experiments, a sperm population size $n \geq 210$ was analyzed in the transverse channels (test zone) of the device for each experimental condition.

Sperm chemotaxis in response to NFA was assessed by estimating the swimming bias in the direction of the gradient generated with 0.01 M NFA. A combined O.R. was calculated for gradient (G/M) and non-gradient (N/M), keeping media control as the baseline. Rest of the analysis was as described in detail in "Material and Methods" section. In addition to this, we also calculated the combined odds for G/N, since non-gradient condition tested here also serves as an indicator of chemokinesis.

Sperm showed an increase in the combined O.R. for 0.01 M NFA gradient (Figure 4B), when compared to its corresponding media and non-gradient control. The absolute numbers of sperm moving left to right and right to left are presented in Table S2. Mean VSL was observed to be significantly higher in the case of sperm population moving along an increasing 0.01 M NFA concentration in comparison to those moving along an decreasing concentration, non-gradient and media control (Figure 4C). This suggests that sperm exhibits a chemotactic response toward 0.01 M NFA. Plotting the frequency distribution curves for NFA, we observed that the sperm population exposed to an increasing gradient of NFA had relatively higher percentage of sperm in the 50–100 μm/s VSL range and a lower percentage in the VSL range of 0–50 μm/s as compared to those exposed to a uniform concentration of NFA or to media. The chemotactic population can be well appreciated with the shift in the peak for 0.01 M NFA gradient as compared to non-gradient and media control (Figure 4D).

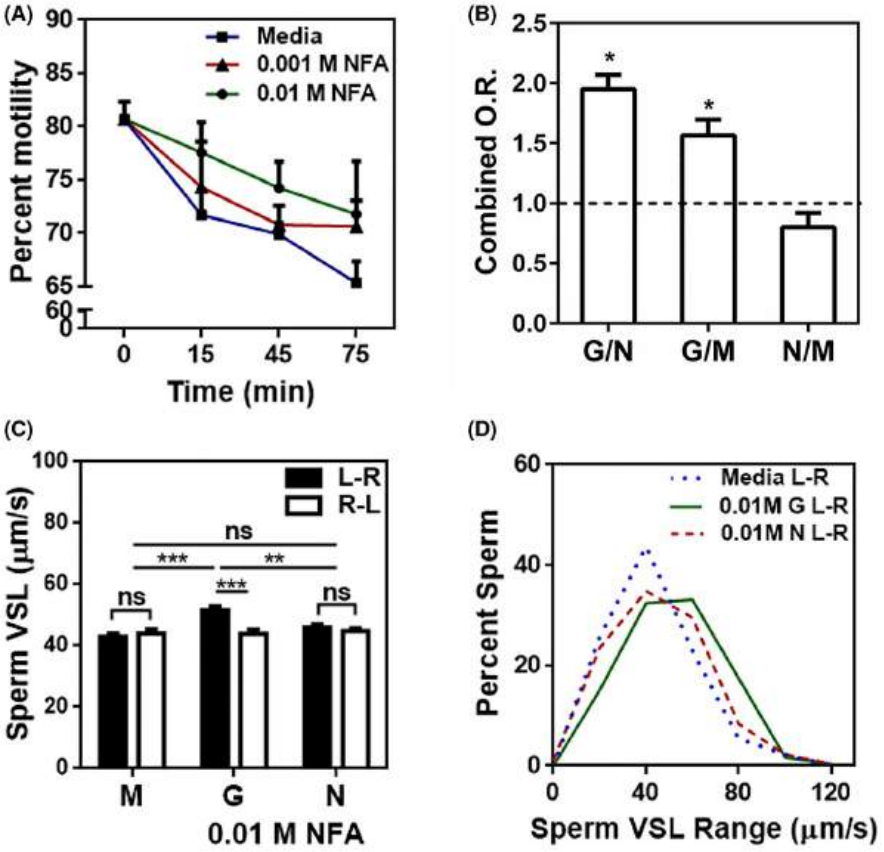

FIGURE 4 Sperm motility and chemotaxis in response to NFA. Sperm motility at 15, 45, and 75 min of incubation of capacitating sperm with 0.01 and 0.001 M NFA (A); Sperm directionality represented by combined odds ratio (O.R.) for the cumulative number of sperm entering the transverse channel for gradient (G) versus non-gradient (N) control (G/N), gradient versus media (M) control (G/M), and non-gradient versus media (N/M) (B); mean VSL (± SEM) for sperm moving from left to right (L-R, black bars) and right to left (R-L, white bars), in the transverse channels (C); VSL frequency distribution (D), in response to an increasing as well as uniform (non-gradient) concentration of 0.01 M NFA ($n = 3$). Sperm exhibit a tendency to travel toward higher NFA concentration (0.01 M) with increased numbers and velocities when compared to the same in media and in NFA non-gradient conditions. "*" $p < 0.05$; "**" $p < 0.005$; "***" $p < 0.0005$.

20472927, 2021, 4, Downloaded from https://onlinelibrary.wiley.com/doi/10.1111/andr.12988 by Icmr - National Institute For Research In Reproductive And Child Health, Wiley Online Library on [27/08/2024]. See the Terms and Conditions (https://onlinelibrary.wiley.com/terms-and-conditions) on Wiley Online Library for rules of use; OA articles are governed by the applicable Creative Commons License

4 | DISCUSSION

Chemotaxis as a guidance mechanism for sperm to reach the oocyte is well established. In the female oviduct/fallopian tube, at the time of ovulation, chemoattractants are released along with the fluid surrounding the COC. These are thought to direct sperm toward the oocyte. We have developed a microfluidic device[12] and demonstrated its utility to study sperm motility behavior in response to a chemotactic source. The next logical step was to determine whether sperm behaved differently in preOV phase milieu versus that in the OV phase. Prior to that, we investigated whether sperm exposure to chemotactic agents triggers an elevated $[Ca^{2+}]_I$ influx, as is well established.[44-47] A dose-dependent $[Ca^{2+}]_I$ influx in sperm was observed on exposure to increasing concentration of OV-OF (Figure 1A). We further compared the $[Ca^{2+}]_I$ levels in sperm in response to preOV- and OV- phase OF and observed that this rise in $[Ca^{2+}]_I$ was seen only in OV-OF (Figure 1B,C). This observation provided a clue to the presence of certain receptors/sensors on the sperm membrane,[46] which may recognize certain components present in OV-OF. Next, we compared sperm chemotactic responses to OV-OF vis-à-vis equal concentration of preOV-OF (0.06 μg/μl). Toward this, we measured the combined O.R. for sperm entering the transverse channels (Figure 2A) in increasing and decreasing concentration gradient of preOV- and OV- OF. We observed enhanced sperm directionality as well as significant increase in the sperm population with increased velocities in the presence of OV-OF (Figure 2B–D). Such a sperm response was not seen toward preOV-OF (Figure 2B–D), suggesting that chemoattractants are present only in the OV-OF. A significantly lower sperm VSL for preOV-OF (Figure 2C) suggests that there may be certain factors present in the preOV-OF which restrain sperm from attaining a VSL of ~40 μm/s as seen in the case of media control. To the best of our knowledge, this is the first study that has systematically compared sperm chemotactic behavior in response to OV- and preOV- OF.

Having noted significant differences in sperm response to OV- and preOV- OF, it was pertinent to identify the constituents in the OV-OF that may likely be responsible for this chemotactic response. Theoretically, a good chemoattractant should have the inherent quality of faster diffusion, and according to Fick's law of diffusion, smaller molecules with greater diffusion coefficient diffuse a larger distance within shorter time. We therefore extracted hydrophilic fractions of OV- and preOV- OF for identifying metabolites from OV-OF and preOV-OF considering the small size and easy diffusibility of chemoattractants in aqueous medium.

Recent studies on the metabolomic differences of FF in female infertility cases,[48–50] in comparison with their controls, and bovine OF[51] isolated from different phases of OV cycle provide clear evidences that metabolites play an important role in female fertility assessment and ovulation. However, there is no information on the "chemoattractants" present amidst these metabolites, as none of these studies were aimed to identify chemoattractants. Hence, we used a metabolomics approach to identify potential hydrophilic metabolites, which might have chemotaxis ability. The metabolites that were either exclusive or increased in OV-OF were studied further, to obtain clues to their biological relevance. Selection of the most promising candidate/s was based on an extensive literature search in PubMed and PubChem for (i) any known functional status, (ii) any reports regarding their presence in OF/FF of any mammalian species and/or (iii) whether the metabolite has been reported to induce chemotaxis in any species, or (iv) whether any of the cognate receptors of the metabolite are involved in chemotaxis. The biological role of certain metabolites that were found to be a qualifier for the above stated criteria is tabulated (Table 3). We focused our attention on NFA for testing its chemotactic potential for several reasons. NFA has been reported as an agonist for β_2-adrenergic receptors,[52] which are G-protein (GP)-coupled receptors (CR) known to activate GP adenylyl cyclase (AC)[53,54] and are strong candidate receptors for chemotaxis.[55] Recent findings with β_2-adrenergic receptor revealed that its activation mobilizes $[Ca^{2+}]_I$ via a non-canonical cAMP-independent signaling pathway, as well.[56] Additionally, β_2-adrenergic receptors[57] and the GP-coupled olfactory receptors[58,59] have been reported to be present on sperm membrane; the latter known to play a major role in chemotaxis.[58] GP-coupled AC is also very important for the regulation of cAMP, a key mediator of sperm motility.[60] In this context, it is important to note that we observed a perceptible increase in sperm motility on incubation with 0.01 M NFA (Figure 4A). This provided the first clue that NFA enhances sperm motility.

Studies have also shown that n-formyl peptides are well known to exhibit chemotaxis in neutrophils.[61] Furthermore, L-aspartic acid was also found to be one of the metabolites decreased in FF of

TABLE 3 Biological relevance of the metabolites exclusive/increased in OV-OF

List of identified metabolites	Functional Significance
N-formyl-L-aspartate	Muscarinic receptor antagonists (PubChem), β2-adrenergic receptor agonists[52] (PubChem) and induce chemotaxis in bacteria[62]
Cinitapride	Gastroprokinetic agent that enhances acetylcholine release from cholinergic receptors[63]
L-gluconate	Progesterone receptor signaling pathway agonist[64]
Leonurine	Anti-inflammatory effects on LPS-induced endometriosis[65]
Cortisone/aldosterone	Steroid hormone[66]
Tetrahydrocolumbamine	Mitochondrial metabolite[67]
Acetoacetyl CoA	Pyruvate metabolism (KEGG)
Oxitropium	Anti-cholinergic bronchodilator[68]

20472927, 2021, 4, Downloaded from https://onlinelibrary.wiley.com/doi/10.1111/andr.12988 by Icmr - National Institute For Research In Reproductive And Child Health, Wiley Online Library on [27/08/2024]. See the Terms and Conditions (https://onlinelibrary.wiley.com/terms-and-conditions) on Wiley Online Library for rules of use; OA articles are governed by the applicable Creative Commons License

women with repeated IVF failures.[48] In addition to this, NFA itself has been reported as a chemoattractant for bacterial species such as *E. coli*.[62] In our study, this compound showed the highest significant difference between the two groups. Thus, NFA being a strong contender for cell motility enhancement, we assessed its role in inducing sperm chemotaxis, using the microfluidic device. Our data demonstrate the chemotaxis-inducing ability of NFA (Figure 4C,D). This is a novel finding. The absence of significant enhancement in sperm mean VSL in NFA non-gradient condition compared to media control and to descending gradient of NFA also shows that NFA does not induce chemokinesis at the concentration tested. Moreover, on measuring sperm response to different gradients of NFA, we observed a bell-shaped curve, as expected for chemotaxis (data not shown). The detection of the attractant probably happens at the entrance of the TC, where sperm sense the lower concentration in the 0.01 M NFA gradient and follow the track to move toward the higher concentrations. Thus, the chemotactic response happens at a much lower dose than 0.01 M which is the concentration at the right end of the TC.

In conclusion, this study has highlighted the differences in metabolomic profiles between OV- and preOV- phases, using the LC-MS/MS approach. A number of putative metabolites were identified and found to exhibit an increase in the OV phase. One of these metabolites (NFA), which was highly significant in terms of its p-value and biologically relevant in terms of chemotaxis, was tested and validated for its ability to induce sperm chemotaxis. We confirmed the role of NFA, as a chemoattractant, using our chemotaxis device. Thus, we have identified a novel chemoattractant for mammalian sperm and proven the utility of the device to test putative chemoattractants. It remains to be seen whether human spermatozoa respond similarly to NFA and if they do, whether NFA is present in the FF of infertile women, and if absent or relatively low, whether it may likely be one of the reasons for the failure of natural conception in idiopathic infertile women. Further studies have been initiated in this direction.

ACKNOWLEDGMENTS

The authors thank the Experimental Animal Facility, ICMR-NIRRH, Mumbai, India. We also thank Dr. Mayuri Gandhi, Ms. Manali Jadhav, and Ms. Pradnya Nikam for performing LC-MS/MS at the Sophisticated Analytical Instrument Facility (SAIF), IIT Bombay (IIT-B), India; the Centre of Excellence for Nanotechnology (CEN), IIT Bombay microfabrication facility; and Ms. Prem Pritam, IIT-B for her assistance during metabolomics data analysis. We also thank Dr. Vivian Lobo, NIRRH for his help in the initial standardization and trouble-shooting of the calcium assay, and Mr. Mahadev Merchande, NIRRH for help with animal handling. This work (RA/915/05-2020) was supported by grants from the Department of Biotechnology (DBT; to P.P. and S.J.; Grant # BT/PR13442/MED/32/440/2015) and core funding from ICMR-NIRRH. The JRF and SRF fellowship provided to S.S (NIRRH) by DBT and SRF to S.B (IIT-B) by DBT and Industrial Research and Consultancy Centre (IRCC), IIT-B is gratefully acknowledged.

CONFLICT OF INTEREST

The authors declare that they have no competing interests.

AUTHOR CONTRIBUTIONS

PP conceptualized the study and SJ conceptualized the microfluidic chemotaxis device for this study. PP, SJ, and SB conceived and designed the experiments. SB performed all experiments and data analysis with the help of SS, while SD and DP helped SB with NFA data analysis. SS, SD, and DP monitored the female rat cyclicity. PP and SJ contributed reagents, materials, and analysis tools. PP and SB wrote the paper, while SJ recommended suggestions to it.

ORCID

Priyanka Parte https://orcid.org/0000-0002-3800-4053

REFERENCES

1. Cohen-Dayag A, Ralt D, Tur-Kaspa I, et al. Sequential acquisition of chemotactic responsiveness by human spermatozoa. *Biol Reprod*. 1994;50(4):786-790. https://doi.org/10.1095/biolreprod50.4.786
2. Cohen-Dayag A, Tur-Kaspa I, Dor J, Mashiach S, Eisenbach M. Sperm capacitation in humans is transient and correlates with chemotactic responsiveness to follicular factors. *Proc Natl Acad Sci U S A*. 1995;92(24):11039-11043. https://doi.org/10.1073/pnas.92.24.11039
3. Koyama S, Amarie D, Soini HA, Novotny MV, Jacobson SC. Chemotaxis assays of mouse sperm on microfluidic devices. *Anal Chem*. 2006;78(10):3354-3359. https://doi.org/10.1021/ac052087i
4. Xie L, Ma R, Han C, et al. Integration of sperm motility and chemotaxis screening with a microchannel-based device. *Clin Chem*. 2010;56(8):1270-1278. https://doi.org/10.1373/clinchem.2010.146902
5. Guidobaldi HA, Teves ME, Uñates DR, Giojalas LC. Sperm transport and retention at the fertilization site is orchestrated by a chemical guidance and oviduct movement. *Reproduction*. 2012;143(5):587-596. https://doi.org/10.1530/REP-11-0478
6. Eisenbach M. Sperm chemotaxis. *Rev Reprod*. 1999;4(1):56-66. https://doi.org/10.1530/ror.0.0040056
7. Eisenbach M, Giojalas LC. Sperm guidance in mammals — an unpaved road to the egg. *Nat Rev Mol Cell Biol*. 2006;7(4):276-285. https://doi.org/10.1038/nrm1893
8. Teves ME, Barbano F, Guidobaldi HA, Sanchez R, Miska W, Giojalas LC. Progesterone at the picomolar range is a chemoattractant for mammalian spermatozoa. *Fertil Steril*. 2006;86(3):745-749. https://doi.org/10.1016/j.fertnstert.2006.02.080
9. Kong N, Xu X, Zhang Y, et al. Natriuretic peptide type C induces sperm attraction for fertilization in mouse. *Sci Rep*. 2017;7:1-12. https://doi.org/10.1038/srep39711
10. Xiang X, Burnett L, Rawls A, Bieber A, Chandler D. The sperm chemoattractant "allurin" is expressed and secreted from the Xenopus oviduct in a hormone-regulated manner. *Dev Biol*. 2004;275(2):343-355. https://doi.org/10.1016/j.ydbio.2004.08.011
11. Ko Y-J, Maeng J-H, Lee B-C, Lee S, Hwang SY, Ahn Y. Separation of progressive motile sperm from mouse semen using on-chip chemotaxis. *Anal Sci*. 2012;28(1):27-32. https://doi.org/10.2116/analsci.28.27
12. Bhagwat S, Sontakke S, Deekshith K, Parte P, Jadhav S. Chemotactic behavior of spermatozoa captured using a microfluidic chip. *Biomicrofluidics*. 2018;12(2):24112. https://doi.org/10.1063/1.5023574

20472927, 2021, 4, Downloaded from https://onlinelibrary.wiley.com/doi/10.1111/andr.12988 by Icmr - National Institute For Research In Reproductive And Child Health, Wiley Online Library on [27/08/2024]. See the Terms and Conditions (https://onlinelibrary.wiley.com/terms-and-conditions) on Wiley Online Library for rules of use; OA articles are governed by the applicable Creative Commons License

13. Caballero-Campo P, Buffone MG, Benencia F, Conejo-García JR, Rinaudo PF, Gerton GL. A role for the chemokine receptor CCR6 in mammalian sperm motility and chemotaxis. *J Cell Physiol*. 2014;229(1):68-78. https://doi.org/10.1002/jcp.24418
14. Sun F, Bahat A, Gakamsky A, et al. Human sperm chemotaxis: both the oocyte and its surrounding cumulus cells secrete sperm chemoattractants. *Hum Reprod*. 2005;20(3):761-767. https://doi.org/10.1093/humrep/deh657
15. Ralt D, Manor M, Cohen-Dayag A, et al. Chemotaxis and chemokinesis of human spermatozoa to follicular factors. *Biol Reprod*. 1994;50(4):774-785. https://doi.org/10.1095/biolreprod50.4.774
16. Oliveira RG, Tomasi L, Rovasio RA, Giojalas LC. Increased velocity and induction of chemotactic response in mouse spermatozoa by follicular and oviductal fluids. *Reproduction*. 1999;115(1):23-27. https://doi.org/10.1530/jrf.0.1150023
17. Serrano H, Canchola E, García-Suárez MD. Sperm-attracting activity in follicular fluid associated to an 8.6-kDa protein. *Biochem Biophys Res Commun*. 2001;283(4):782-784. https://doi.org/10.1006/bbrc.2001.4861
18. Fabro G, Rovasio RA, Civalero S, et al. Chemotaxis of capacitated rabbit spermatozoa to follicular fluid revealed by a novel directionality-based assay. *Biol Reprod*. 2002;67(5):1565-1571. https://doi.org/10.1095/biolreprod.102.006395
19. Guidobaldi HA, Hirohashi N, Cubilla M, Buffone MG, Giojalas LC. An intact acrosome is required for the chemotactic response to progesterone in mouse spermatozoa. *Mol Reprod Dev*. 2017;84(4):310-315. https://doi.org/10.1002/mrd.22782
20. Guidobaldi HA, Teves ME, Unates DR, Anastasia A, Giojalas LC. Progesterone from the cumulus cells is the sperm chemoattractant secreted by the rabbit oocyte cumulus complex. *PLoS One*. 2008;3(8):1-9. https://doi.org/10.1371/journal.pone.0003040
21. Armon L, Ben-Ami I, Ron-El R, Eisenbach M. Human oocyte-derived sperm chemoattractant is a hydrophobic molecule associated with a carrier protein. *Fertil Steril*. 2014;102(3):885-890. https://doi.org/10.1016/j.fertnstert.2014.06.011
22. Sliwa L. Effect of heparin on human spermatozoa migration in vitro. *Arch Androl*. 1993;30(3):177-181. https://doi.org/10.3109/01485019308987754
23. Šliwa L. Chemotactic effect of hormones in mouse spermatozoa. *Arch Androl*. 1994;32(2):83-88. https://doi.org/10.3109/01485019408987772
24. Sliwa L. Chemotaction of mouse spermatozoa induced by certain hormones. *Arch Androl*. 1995;35(2):105-110. https://doi.org/10.3109/01485019508987860
25. Śliwa L. Effect of some sex steroid hormones on human spermatozoa migration in vitro. *Eur J Obstet Gynecol Reprod Biol*. 1995;58(2):173-175. https://doi.org/10.1016/0028-2243(95)80019-O
26. Pérez-Cerezales S, Boryshpolets S, Eisenbach M. Behavioral mechanisms of mammalian sperm guidance. *Asian J Androl*. 2015;17(4):628. https://doi.org/10.4103/1008-682X.154308
27. Bian F, Mao G, Guo M, et al. Gradients of natriuretic peptide precursor A (NPPA) in oviduct and of natriuretic peptide receptor 1 (NPR1) in spermatozoon are involved in mouse sperm chemotaxis and fertilization. *J Cell Physiol*. 2012;227(5):2230-2239. https://doi.org/10.1002/jcp.22962
28. Hino T, Yanagimachi R. Active peristaltic movements and fluid production of the mouse oviduct: Their roles in fluid and sperm transport and fertilization. *Biol Reprod*. 2019;101(1):240-249. https://doi.org/10.1093/biolre/ioz061
29. Hubscher C, Brooks D, Johnson J. A quantitative method for assessing stages of the rat estrous cycle. *Biotech Histochem*. 2005;80(2):79-87. https://doi.org/10.1080/10520290500138422
30. Seed J, Chapin RE, Clegg ED, et al. Methods for assessing sperm motility, morphology, and counts in the rat, rabbit, and dog: a consensus report. *Reprod Toxicol*. 1996;10(3):237-244. https://doi.org/10.1016/0890-6238(96)00028-7
31. Grynkiewicz G, Poenie M, Tsien RY. A new generation of Ca2+ indicators with greatly improved fluorescence properties. *J Biol Chem*. 1985;260(6):3440-3450.
32. Lobo V, Parte P. Membrane-bound Glucose regulated protein 78 interacts with alpha-2-macroglobulin to promote actin reorganization in sperm during epididymal maturation. *Mol Hum Reprod*. 2019;25(3):137-155. https://doi.org/10.1093/molehr/gay055
33. Morris JA, Gardner MJ. Statistics in Medicine: Calculating confidence intervals for relative risks (odds ratios) and standardised ratios and rates. *Br Med J*. 1988;296(6632):1313-1316. https://doi.org/10.1136/bmj.296.6632.1313
34. Armon L, Caplan SR, Eisenbach M, Friedrich BM. Testing human sperm chemotaxis: how to detect biased motion in population assays. *PLoS One*. 2012;7(3):e32909. https://doi.org/10.1371/journal.pone.0032909
35. Schneider CA, Rasband WS, Eliceiri KW. NIH Image to ImageJ: 25 years of image analysis. *Nat Methods*. 2012;9(7):671-675. https://doi.org/10.1038/nmeth.2089
36. Nakayasu ES, Nicora CD, Sims AC, et al. MPLEx: a robust and universal protocol for single-sample integrative proteomic, metabolomic, and lipidomic analyses. *mSystems*. 2016;1(3):e00043-e116. https://doi.org/10.1128/mSystems.00043-16
37. Sana TR, Gordon DB, Fischer SM, et al. Global mass spectrometry based metabolomics profiling of erythrocytes infected with *Plasmodium falciparum*. *PLoS One*. 2013;8(4):e60840. https://doi.org/10.1371/journal.pone.0060840
38. Chambers MC, Maclean B, Burke R, et al. A cross-platform toolkit for mass spectrometry and proteomics. *Nat Biotechnol*. 2012;30(10):918-920. https://doi.org/10.1038/nbt.2377
39. Tautenhahn R, Patti GJ, Rinehart D, Siuzdak G. XCMS online: a web-based platform to process untargeted metabolomic data. *Anal Chem*. 2012;84(11):5035-5039. https://doi.org/10.1021/ac300698c
40. Gowda H, Ivanisevic J, Johnson CH, et al. Interactive XCMS online: simplifying advanced metabolomic data processing and subsequent statistical analyses. *Anal Chem*. 2014;86(14):6931-6939. https://doi.org/10.1021/ac500734c
41. Forsberg EM, Huan T, Rinehart D, et al. Data processing, multi-omic pathway mapping, and metabolite activity analysis using XCMS Online. *Nat Protoc*. 2018;13(4):633-651. https://doi.org/10.1038/nprot.2017.151
42. Chong J, Soufan O, Li C, et al. MetaboAnalyst 4.0: towards more transparent and integrative metabolomics analysis. *Nucleic Acids Res*. 2018;46(W1):W486-W494. https://doi.org/10.1093/nar/gky310
43. Smith CA, Want EJ, O'Maille G, Abagyan R, Siuzdak G. XCMS: Processing mass spectrometry data for metabolite profiling using nonlinear peak alignment, matching, and identification. *Anal Chem*. 2006;78(3):779-787. https://doi.org/10.1021/ac051437y
44. Cook SP, Brokaw CJ, Muller CH, Babcock DF. Sperm chemotaxis: Egg peptides control cytosolic calcium to regulate flagellar responses. *Dev Biol*. 1994;165(1):10-19. https://doi.org/10.1006/dbio.1994.1229
45. Wood CD, Darszon A, Whitaker M. Speract induces calcium oscillations in the sperm tail. *J Cell Biol*. 2003;161(1):89-101. https://doi.org/10.1083/jcb.200212053
46. Baldi E, Casano R, Falsetti C, Krausz C, Maggi M, Gianni F. Intracellular calcium accumulation and responsiveness to progesterone in capacitating human spermatozoa. *J Androl*. 1991;12(5):323-330.
47. Strünker T, Goodwin N, Brenker C, et al. The CatSper channel mediates progesterone-induced Ca2+ influx in human sperm. *Nature*. 2011;471(7338):382-386. https://doi.org/10.1038/nature09769
48. Xia L, Zhao X, Sun Y, Hong Y, Gao Y, Hu S. Metabolomic profiling of human follicular fluid from patients with repeated failure of in vitro fertilization using gas chromatography / mass spectrometry. *Int J Clin Exp Pathol*. 2014;7(10):7220-7229.

20472927, 2021, 4, Downloaded from https://onlinelibrary.wiley.com/doi/10.1111/andr.12988 by Icmr - National Institute For Research In Reproductive And Child Health, Wiley Online Library on [27/08/2024]. See the Terms and Conditions (https://onlinelibrary.wiley.com/terms-and-conditions) on Wiley Online Library for rules of use; OA articles are governed by the applicable Creative Commons License

49. Marianna S, Alessia P, Susan C, et al. Metabolomic profiling and biochemical evaluation of the follicular fluid of endometriosis patients. *Mol Biosyst*. 2017;13(6):1213-1222. https://doi.org/10.1039/C7MB00181A
50. Cordeiro FB, Cataldi TR, do Vale Teixeira da Costa L, et al. Metabolomic profiling in follicular fluid of patients with infertility-related deep endometriosis. *Metabolomics*. 2017;13(10):120. https://doi.org/10.1007/s11306-017-1262-3
51. Lamy J, Gatien J, Dubuisson F, et al. Metabolomic profiling of bovine oviductal fluid across the oestrous cycle using proton nuclear magnetic resonance spectroscopy. *Reprod Fertil Dev*. 2018;30(7):1021. https://doi.org/10.1071/RD17389
52. Choi S-K, Moran EJ. β2-adrenergic receptor agonists US7427639. Published online 2008. doi:US 20070179179 A1.
53. Galandrin S, Bouvier M. Distinct signaling profiles of β 1 and β 2 adrenergic receptor ligands toward adenylyl cyclase and mitogen-activated protein kinase reveals the pluridimensionality of efficacy. *Mol Pharmacol*. 2006;70(5):1575-1584. https://doi.org/10.1124/mol.106.026716
54. Johnson M. Molecular mechanisms of β2-adrenergic receptor function, response, and regulation. *J Allergy Clin Immunol*. 2006;117(1):18-24. https://doi.org/10.1016/j.jaci.2005.11.012
55. Eisenbach M. Towards understanding the molecular mechanism of sperm chemotaxis. *J Gen Physiol*. 2004;124(2):105-108. https://doi.org/10.1085/jgp.200409142
56. Galaz-Montoya M, Wright SJ, Rodriguez GJ, Lichtarge O, Wensel TG. β 2 -Adrenergic receptor activation mobilizes intracellular calcium via a non-canonical cAMP-independent signaling pathway. *J Biol Chem*. 2017;292(24):9967-9974. https://doi.org/10.1074/jbc.M117.787119
57. Adeoya-Osiguwa SA, Gibbons R, Fraser LR. Identification of functional α2- and β-adrenergic receptors in mammalian spermatozoa. *Hum Reprod*. 2006;21(6):1555-1563. https://doi.org/10.1093/humrep/del016
58. Walensky LD, Roskams AJ, Lefkowitz RJ, Snyder SH, Ronnett GV. Odorant receptors and desensitization proteins colocalize in mammalian sperm. *Mol Med*. 1995;1(2):130-141. https://doi.org/10.1007/BF03401561
59. Spehr M, Schwane K, Riffell JA, et al. Particulate adenylate cyclase plays a key role in human sperm olfactory receptor-mediated chemotaxis. *J Biol Chem*. 2004;279(38):40194-40203. https://doi.org/10.1074/jbc.M403913200
60. Esposito G, Jaiswal BS, Xie F, et al. Mice deficient for soluble adenylyl cyclase are infertile because of a severe sperm-motility defect. *Proc Natl Acad Sci*. 2004;101(9):2993-2998. https://doi.org/10.1073/pnas.0400050101
61. Naccache PH, Therrien S, Caon AC, Liao N, Gilbert C, McColl SR. Chemoattractant-induced cytoplasmic pH changes and cytoskeletal reorganization in human neutrophils. Relationship to the stimulated calcium transients and oxidative burst. *J Immunol*. 1989;142(7):2438-2444.
62. Bi S, Yu D, Si G, et al. Discovery of novel chemoeffectors and rational design of Escherichia coli chemoreceptor specificity. *Proc Natl Acad Sci*. 2013;110(42):16814-16819. https://doi.org/10.1073/pnas.1306811110
63. Massingham R, Bou J, Roberts DJ. A comparison of the simulatory effects of metoclopramide and cinitapride in the Guinea-pig isolated ileum. *J Auton Pharmacol*. 1985;5(1):41-53. https://doi.org/10.1111/j.1474-8673.1985.tb00564.x
64. Wistrom CA, Meizel S. Evidence suggesting involvement of a unique human sperm steroid receptor/Cl- channel complex in the progesterone-initiated acrosome reaction. *Dev Biol*. 1993;159(2):679-690. https://doi.org/10.1006/dbio.1993.1274
65. Wu H, Dai A, Chen X, et al. Leonurine ameliorates the inflammatory responses in lipopolysaccharide-induced endometritis. *Int Immunopharmacol*. 2018;61:156-161. https://doi.org/10.1016/j.intimp.2018.06.002
66. Holst JP, Soldin OP, Guo T, Soldin SJ. Steroid hormones: relevance and measurement in the clinical laboratory. *Clin Lab Med*. 2004;24(1):105-118. https://doi.org/10.1016/j.cll.2004.01.004
67. Marques AP, Serralheiro ML, Ferreira AEN, Freire AP, Cordeiro C, Silva MS. Metabolomics for undergraduates: identification and pathway assignment of mitochondrial metabolites. *Biochem Mol Biol Educ*. 2016;44(1):38-54. https://doi.org/10.1002/bmb.20919
68. Cazzola M, Matera MG, Di Perna F, Calderaro F, Califano C, Vinciguerra A. A comparison of bronchodilating effects of salmeterol and oxitropium bromide in stable chronic obstructive pulmonary disease. *Respir Med*. 1998;92(2):354-357. https://doi.org/10.1016/S0954-6111(98)90121-4

SUPPORTING INFORMATION

Additional supporting information may be found online in the Supporting Information section.

How to cite this article: Bhagwat S, Sontakke S, Desai S, Panchal D, Jadhav S, Parte P. N-formyl-L-aspartate: A novel sperm chemoattractant identified in ovulatory phase oviductal fluid using a microfluidic chip. *Andrology*. 2021;9:1214–1226. https://doi.org/10.1111/andr.12988

20472927, 2021, 4, Downloaded from https://onlinelibrary.wiley.com/doi/10.1111/andr.12988 by Icmr - National Institute For Research In Reproductive And Child Health, Wiley Online Library on [27/08/2024]. See the Terms and Conditions (https://onlinelibrary.wiley.com/terms-and-conditions) on Wiley Online Library for rules of use; OA articles are governed by the applicable Creative Commons License